AD-A173 683 NON-INVASIVE ELECTRO-MAGNETIC FIELD SENSOR(U) 1/1
GEO-CENTERS INC NEWTON CENTRE MA B W NELSON ET AL.
JAN 86 GC-TR-578-01 AFWAL-TR-86-3051 F33615-85-C-3417
UNCLASSIFIED F/G 14/2 NL

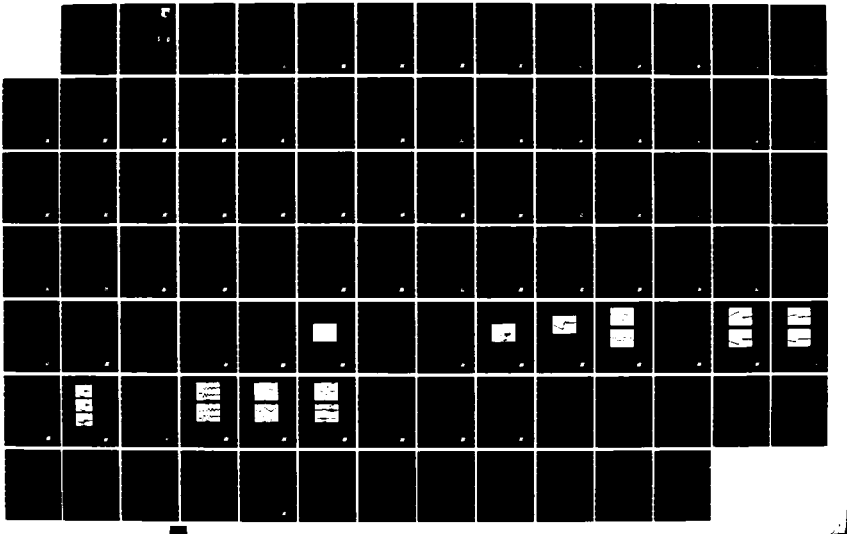

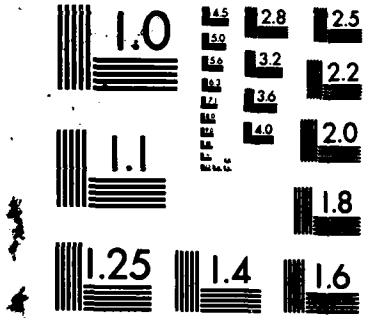

MICROCOPY RESOLUTION TEST CHART
NATIONAL BUREAU OF STANDARDS-1963-A

AD-A173 683

AFWAL-TR-86-3051

NON-INVASIVE ELECTRO-MAGNETIC FIELD SENSOR

Bruce N. Nelson, Christoph Menzel and Thomas G. DiGuisseppe

Geo-Centers, Inc.
7 Wells Avenue
Newton Centre, MA 02159

DTIC
ELECTE
OCT 3 0 1986
S D
D

January 1986

Final Report for Period May 1985 - May 1986

DTIC FILE COPY

Approved for public release; distribution unlimited.

FLIGHT DYNAMICS LABORATORY
AIR FORCE WRIGHT AERONAUTICAL LABORATORIES
AIR FORCE SYSTEMS COMMAND
WRIGHT-PATTERSON AIR FORCE BASE, OHIO 45433-6553

86 10 30 045

UNCLASSIFIED

SECURITY CLASSIFICATION OF THIS PAGE

AD-A173 683

REPORT DOCUMENTATION PAGE

1a. REPORT SECURITY CLASSIFICATION UNCLASSIFIED	1b. RESTRICTIVE MARKINGS N/A
2a. SECURITY CLASSIFICATION AUTHORITY N/A	3. DISTRIBUTION/AVAILABILITY OF REPORT Approved for public release; distribution unlimited.
2b. DECLASSIFICATION/DOWNGRADING SCHEDULE N/A	
4. PERFORMING ORGANIZATION REPORT NUMBER(S) GC-TR-578-01	5. MONITORING ORGANIZATION REPORT NUMBER(S) AFWAL-TR-86-3051
6a. NAME OF PERFORMING ORGANIZATION Geo-Centers, Inc. 6b. OFFICE SYMBOL (If applicable)	7a. NAME OF MONITORING ORGANIZATION Flight Dynamics Laboratory (AFWAL/FIESL)
6c. ADDRESS (City, State and ZIP Code) 7 Wells Avenue Newton Centre, MA 02159	7b. ADDRESS (City, State and ZIP Code) Air Force Wright Aeronautical Laboratories (AFSC) Wright-Patterson AFB, OH 45433
8a. NAME OF FUNDING/SPONSORING ORGANIZATION Aeronautical Systems Division 8b. OFFICE SYMBOL (If applicable) ASD	9. PROCUREMENT INSTRUMENT IDENTIFICATION NUMBER Contract No. F33615-85-3417
8c. ADDRESS (City, State and ZIP Code) Wright-Patterson AFB, OH 45433 (AFSC)	10. SOURCE OF FUNDING NOS. PROGRAM ELEMENT NO. 65502F; PROJECT NO. 3005; TASK NO. 30; WORK UNIT NO. 38
11. TITLE (Include Security Classification) (UNCLASSIFIED) Non-Invasive Electro-Magnetic Field Sensor	
12. PERSONAL AUTHOR(S) Nelson, Bruce N.; Menzel, Christoph; and DiGiusseppe, Thomas G.	
13a. TYPE OF REPORT Final 13b. TIME COVERED FROM May 85 TO May 86	14. DATE OF REPORT (Yr., Mo., Day) January 1986 15. PAGE COUNT 92
16. SUPPLEMENTARY NOTATION Small Business Innovation Research (SBIR) Phase I Report	

17. COSATI CODES		
FIELD	GROUP	SUB. GR.
14	02	
04	01	

18. SUBJECT TERMS (Continue on reverse if necessary and identify by block number)
Electromagnetic Field Sensor; Electric Field; Electromagnetic Measurements; Electro-optic Crystal; Fiber Optic Sensor; Non-invasive Sensor

19. ABSTRACT (Continue on reverse if necessary and identify by block number)

The development of a non-invasive electromagnetic field sensor that would not perturb the electric field being measured was investigated. Electro-optic crystals were selected such that a difference in the index of refraction along the optical axes would result in a change in transmission through the optical system when an electric field was applied. Through the choice of appropriate crystals and crystal geometries, various sensitivities and AC bandwidths are attained in a fiber optic sensor. The electro-optic effect exhibited in electro-optic crystals is sensitive to an electric field in only one direction. A sensor can be developed using multiple crystals mounted orthogonally that can measure both the strength and direction of the electric field. The electronics and signal processing equipment can be located a great distance from the sensor allowing for real time electric field measurements in hostile environments. This phase of research was directed towards selecting suitable electro-optic crystals for the design of such a sensor and towards determining the optimum means of signal detection.

20. DISTRIBUTION/AVAILABILITY OF ABSTRACT UNCLASSIFIED/UNLIMITED ☒ SAME AS RPT. ☐ DTIC USERS ☐	21. ABSTRACT SECURITY CLASSIFICATION UNCLASSIFIED
22a. NAME OF RESPONSIBLE INDIVIDUAL 1Lt Harold D. Burket	22b. TELEPHONE NUMBER (Include Area Code) (513) 257-7718 22c. OFFICE SYMBOL AFWAL/FIESL

DD FORM 1473, 83 APR EDITION OF 1 JAN 73 IS OBSOLETE.

UNCLASSIFIED

SECURITY CLASSIFICATION OF THIS PAGE

DOD No. 85.1

U.S. DEPARTMENT OF DEFENSE

SMALL BUSINESS INNOVATION RESEARCH PROGRAM
PHASE 1 – FY 1985
PROJECT SUMMARY

Topic No. 33 Military Department/Agency Air Force

Name and Address of Proposer

GEO-CENTERS, INC.
320 Needham Street
Newton Upper Falls, MA 02164

Name and Title of Principal Investigator

Bruce N. Nelson, Senior Optical Engineer

Proposer's Title*

NON-INVASIVE ELECTROMAGNETIC FIELD SENSOR

Technical Abstract* (Limit your abstract to 200 words with no classified or proprietary information/data.)

The development of a non-intrusive electric field sensor based on the electro-optic effect is proposed. Electro-optic crystals are selected such that a difference in the index of refraction along the principal optical axes, induced by a changing electric field, results in a change in transmission through the optical system. Through the choice of an appropriate crystal and crystal geometries, various sensitivities and AC bandwidths are attained in a fiber optic sensor. The nature of the electro-optic effect exhibited in electro-optic crystals selects sensitivities to the electric field only in one direction. Therefore, a sensor can be developed with 3 electro-optic crystals mounted orthogonally such that both field strength and direction can be determined. Also, the electronics and signal processing equipment are located at a great distance from the sensor end, allowing for real time electric field measurements in hostile environments. Phase I research is directed at the selection of suitable electro-optic crystals for designing fiber optic sensors and towards the determination of optimum means of signal detection.

Anticipated Benefits/Potential Commercial Applications of the Research or Development

Successful completion of Phase I and II research programs results in a small, lightweight, real-time electric field sensor capable of measuring both strength and direction of electric fields in hostile environments. This would make it an ideal sensor for measurements in the lightning research area. With the development of radiation hardened fibers and/or sum-difference output detection schemes, the sensor would also be ideal for NEMP measurements.

List a maximum of 8 Key Words that describe the Project.

Electric Fields Electro-Optic Crystals

Fiber Optic Sensors

*Nothing on this page is classified or proprietary information/data

GEO-CENTERS, INC.

TABLE OF CONTENTS

Section			Page
List of Figures			vi
List of Tables			viii
1.0	Executive Summary		3
2.0	Introduction and Identification of the Problem		6
	2.1	Technical Approach	8
	2.2	Comparison of Electro-Optic Cyrstals for Electric Field Sensors	19
3.0	Phase I Results		22
	3.1	Summary	22
	3.2	Theory	22
	3.3	Experimental Results	34
		3.3.1 Instrumentation	34
		3.3.2 Response to Applied Electric Fields	38
		3.3.2.1 D.C. Measurements	38
		3.3.2.1.1 BGO	41
		3.3.2.1.2 KDP	50
		3.3.2.2 A.C. Measurements	53
		3.3.3 Results from Tests at AFWAL/FIESL Facility	70
4.0	Conclusions & Recommendations		82
Appendix A			85
References			88

QUALITY INSPECTED 1

Accesion For
NTIS CRA&I
DTIC TAB
Unannounced
Justification
By
Distribution/
Availability Codes
Dist Avail and/or Special
A-1

GEO-CENTERS, INC.

LIST OF FIGURES

Figure		Page
1	The optical components and their orientation for a fiber optic electric field sensor	10
2	Orientation of fast and slow axes in BGO crystals for electric fields applied along the <001> and the <110> crystal directions	13
3	Two optical axes in one crystal	14
4	Crystal orientations for a 3-axis electric field sensor utilizing BGO electro-optic crystal (X direction is redundant)	16
5	Crystal orientations	27
6	Axes rotation	28
7	Axes orientation with applied electric fields	32
8	GEO-CENTERS, INC.'s ellipsometer	35
9	MERET pin diode circuit	39
10	Experimental setup for DC measurements	40
11	Changes in transmission versus applied field for the two indpendent polarization states for 5 mm BGO	42
12	Change in transmission versus applied field for 5 mm BGO crystal	44
13	Change in transmission versus applied field for 5 mm BGO crystal	45
14	Comparison of transmission change for three different crystal lengths in BGO	46
15	Change in transmission versus applied electric field in BGO	47
16	Change in transmission versus applied electric field in BGO	48

17 Change in transmission versus applied field in BGO..... 49

18 Observed output fluctuations in KDP crystal. No electric field applied..... 51

19 Depolarization effect..... 52

20 Voltage applied to the parallel plates..... 55

21 Experimental setup for AC measurements..... 56

22 Sensor's response to pulsed electric fields..... 58

23 Results from five superimposed tests..... 59

24 Representative optical biasing information..... 60

25 5 mm sensor's response to electric field pulse..... 62

26 5 mm sensor's response to electric field pulse..... 63

27 A comparison of the response of different length crystals to the same pulse in BGO..... 65

28 Sensor and probe response to applied pulse..... 67

29 20 mm crystal's response to low-level oscillating fields. 68

29 20 mm crystal's response to low-level oscillating fields. 69

30 Fiber optic sensor's response to a pulsed electric field. 74

31 Fiber optic electric field sensor's response to an oscillatory field..... 76

32 Fiber optic sensor's response to parallel plate discharge 78

33 Results from test to characterize GEO-CENTERS's photodetector system..... 79

LIST OF TABLES

Table		Page
1	Crystal Geometries Incorporated for D.C. Electric Field Tests	41
2	Optical Biasing Information	57
3	Tabulated Results from A.C. Electric Field Measurements	61
4	The Effects of Crystal Length on A.C. Measurement Response	64

GEO CENTERS, INC.

1.0 Executive Summary

The goal of the Phase I research effort was to determine the feasibility of using an electro-optic crystal as a sensing element in a fiber optic electric field sensor. This goal has been achieved by the successful completion of each of the tasks outlined in the Phase I Statement of Work. Further development will result in fiber optic electric field sensors with measurement capabilities which are applicable to both Nuclear Electro-Magnetic Pulse (NEMP) and lightning research areas.

A sensor utilizing this technology is completely dielectric in composition so that perturbation to the electric field being measured would be minimal. The output from such a sensor is a direct measurement of the applied electric field along a particular direction. These two sensor properties make a fiber optic electric field sensor based on the electro-optic effect clearly superior to the $\dot{D}$ electric field sensors presently used in lightning research ($\dot{D}$ electric field sensors cause perturbations in the field being measured and their outputs have to be integrated to determine the applied electric field).

The nature of the electro-optic effect exhibited in certain electro-optic crystals allows for the selection of electric field sensitivities in only one direction. This direction is determined by the orientation of polarizing optics used in the fiber optic electric field sensor. By incorporating two optical axes and polarizer orientations in a single electro-optic crystal, two electric field sensors with orthogonal directional sensitivities can be created. This allows a sensor to be developed with two

electro-optic crystals mounted orthogonally such that both electric field strength and direction can be determined (3 axis electric field measurement).

Fiber optic technology also allows the sensor electronics and signal processing equipment to be located at great distances from the electric field being measured. This allows for real time electric field measurements in hostile environments. The utilization of a sum-difference output detection scheme results in a fiber optic electric field sensor whose output is transmitted intensity invariant. The development of a fiber optic electric field sensor which could operate in a nuclear environment is then possible as the effects of radiation fiber darkening minimally affect the sensor's output.

Experimental results are presented which show the feasibility of utilizing a $Bi_4(GeO_4)_3$ (BGO) electro-optic crystal as a sensing element in a fiber optic electric field sensor for lightning research. The data presented demonstrate a linear sensing range between 10^2 V/m and 10^7 V/m and A.C. measurement bandwidth capabilities of at least 10 MHz. With the further development of our sensor electronics and A.C. electric field generating equipment, linear sensing ranges between 1 V/m and 10^7 V/m, and an A.C. measurement bandwidth capability well in excess of 100 MHz should be achievable. This development is straight forward and is based on the use of state of the art high bandwidth circuitry in the sensor electronics. These electric field measurements, utilizing BGO as a sensing element, will result in a fiber optic electric field sensor uniquely suited to the needs of the lightning research area.

A prototype fiber optic electric field sensor utilizing a BGO crystal was designed, fabricated, and tested during this Phase I research effort. These tests were performed at Wright Patterson Air Force Base in Dayton, Ohio, in conjunction with personnel from the Air Force Wright Aeronautical Laboratories Lightning Research Group. This work demonstrates that the technology developed in the laboratory at GEO-CENTERS, INC. with bulk optics can be utilized in a fiber optic sensor. Results from these tests are also presented in this report.

The Phase I research effort described in this report clearly demonstrates that a fiber optic electric field sensor which utilizes BGO as a sensing element is a viable electric field sensor for lightning research applications.

2.0 Introduction and Identification of the Problem

There exists a need to provide survivable electric field sensors which are capable of operating in hostile environments for research in the Nuclear Electro-Magnetic Pulse (NEMP) and lightning areas. Fiber optic technology provides the possibility of monitoring electric fields in real time, in the hostile environments encountered in NEMP measurements, and lightning research. A multi-mode fiber optic sensor has been designed at GEO-CENTERS, INC. which incorporates electro-optic crystals and polarization optics and which is capable of measuring electric field strength, direction, and A.C. characteristics in the environments previously mentioned. A prototype multi-mode fiber optic electric field sensor has been fabricated and tested by GEO-CENTERS, INC. which is capable of single axis electric field measurements in the environment encountered in lightning research.

The Phase I research effort concentrated on the development of an electric field sensor for lightning research where a linear sensing range between $1x10^2$ V/m and $3x10^6$ V/m, and an A.C. measurement bandwidth capability of approximately 10 MHz are required. A sensor for this application should not perturb the electric field to be measured, should have the capability of measuring electric field direction, and be relatively small so that arrays of sensors can be deployed over large objects (such as airplane fuselages) for electric field gradient and distribution measurements.

For NEMP measurements, an electric field sensor should have a linear sensing range between $1x10^2$ V/m and $1x10^7$ V/m and an A.C. measurement bandwidth capability which approaches a GHz. A sensor for this application must also be capable of operating in a nuclear environment which will expose it to gamma rays, x-rays, and

high energy particles.

Presently, $\dot{D}$ sensors, which are available from EG&G Washington Analytical Services Center, Inc., are utilized in lightning and NEMP research applications. These sensors are capacitive in nature and do not measure the applied electric field directly, but instead measure the time derivative of the electric field displacement. Hence, the output of these sensors has to be integrated over time to determine the applied electric field. These sensors are also fabricated with metallic components which causes a distortion of the electric field to be measured. These sensors are sensitive to electric fields in a single direction and are not easily utilized in making electric field directional measurements from a single location. These sensors require, in many applications, electrical to optical converters to prevent the collected data from being compromised in a coaxial cable due to the effects of Electro-Magnetic Interference (EMI).

A fiber optic electric field sensor based on the electro-optic effect can be designed to meet both lightning and NEMP measurement requirements. GEO-CENTERS, INC. has demonstrated a linear sensing range of between $1x10^2$ V/m and $1x10^7$ V/m, and an A.C. measurement bandwidth capability in excess of 10 MHz in an optical sensor based on the electro-optic effect in a $Bi_4(GeO_4)_3$ (BGO) electro-optic crystal. With improvements in the optical source and optical detectors incorporated, a linear sensing range between 1 V/m and $1x10^7$ V/m, and an A.C. measurement bandwidth capability approaching a GHz should be realized. These improvements are straight forward and involve the use of state of the art high bandwidth circuitry in the sensor electronics. This sensor can be fabricated entirely with dielectric materials so that

minimal perturbation occurs to the electric field being measured. In the sensor configuration defined in Section 2.1, uni-axial electric field sensitivity is achieved. As a result of the small size of the crystals employed (<2cm), a sensor head, which incorporates multiple crystals, can be configured in a two inch cube and can measure both electric field strength and direction (3 axes). In addition, sum-difference output detection schemes result in an optical sensor which is relatively immune to the effects of radiation fiber darkening which might be encountered in NEMP measurements. The monitoring of both output polarization states gives a transmitted intensity invariant sensor output resulting in immunity to darkening. Regardless of the sensor output detection scheme, the sensor output is a direct measure of the applied electric field. This allows for electric field measurements without the need for sensor output integration.

In addition, this sensor does not require electrical to optical converters which are utilized with the D sensors to avoid the effects of EMI. Fiber lengths greater than 100 meters can be incorporated between the sensing heads and the optical source and detector which allows all of the sensor system's electronics and signal processing equipment to be located in a non-hostile environment.

These characteristics make a fiber optic electric field sensor based on the electro-optic effect uniquely suited for measurement applications in the NEMP and lightning research areas.

2.1 Technical Approach

The application of an electric field to an electro-optic crystal results in a change in refractive index along certain

crystal directions. In certain electro-optic crystals when an electric field is applied along a specific crystallographic direction, the resultant refractive indices are different for orthogonal directions in the crystal. If light is initially polarized at $\pi/4$ with respect to these different refractive index directions, then a phase shift will occur between the two components of the polarized light that lie along each of these crystal directions as the light propagates through the crystal. This phase shift is proportional to the applied electric field strength and is referred to as electrically induced birefringence, resulting from the electro-optic effect.

The electro-optic effect can be utilized in a fiber optic sensor in order to detect electric field strength. Figure 1 shows a schematic layout of the components and their orientations for a fiber optic electric field sensor. When an electric field is applied along the x direction, the index of refraction increases along that direction, while the index of refraction along the y direction remains constant. A beam polarized along the x axis propagates at a slower speed than a beam which is polarized along the y axis. Consequently, the x axis is known as the slow axis and the y axis is known as the fast axis. Consider first the optical configuration shown in Figure 1 with the 1/4 wave plate removed. For this case, collimated light from the optical source passes through a polarizer oriented at $\pi/4$ with respect to the x-y plane. When an electric field is applied parallel to the x axis, a phase shift occurs between the components of light along the x and y axis (birefringence). This induced birefringence causes the light which exits the crystal and is nominally linearly polarized at $\pi/4$ with respect to the x-y plane, to become elliptically polarized, then circularly polarized, then elliptically polarized, and finally linearly polarized at $-\pi/4$ with respect to the x-y

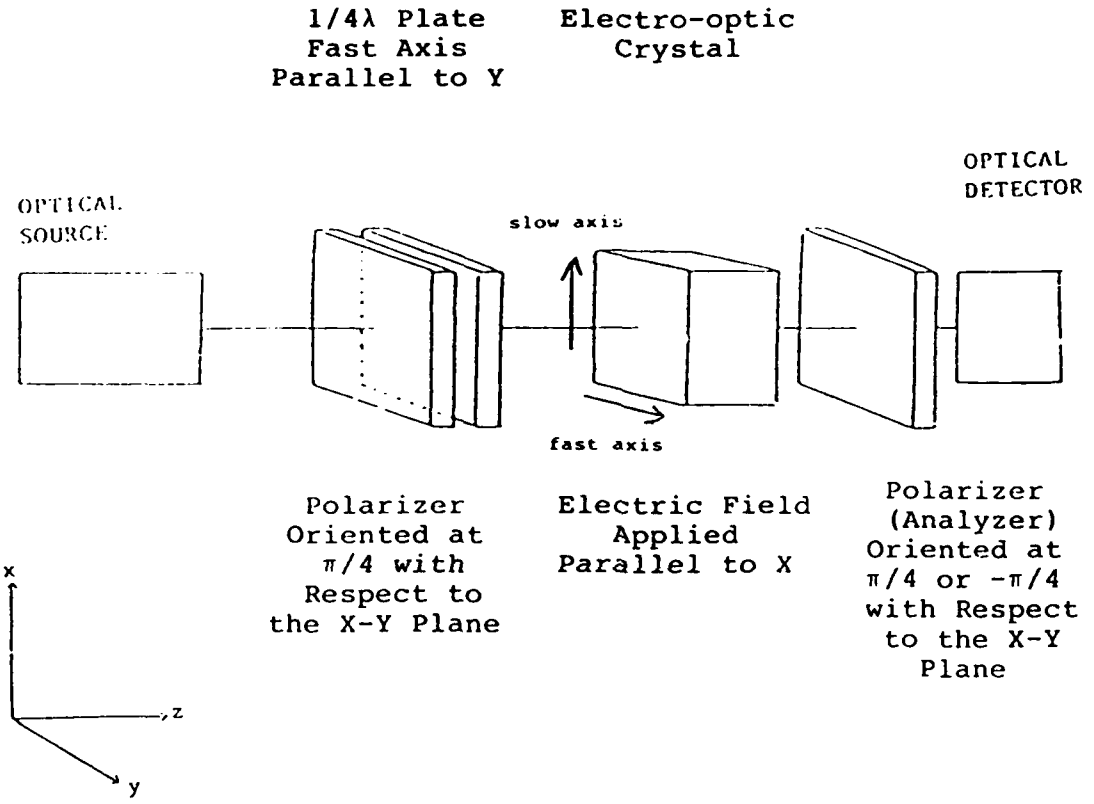

Figure 1. The optical components and their orientation for a fiber optic electric field sensor.

plane. Because of this, two different orientations for the final polarizer (analyzer) are of interest, these being $+\pi/4$ and $-\pi/4$ with respect to the x-y plane.

The optical intensity that reaches the detectors exhibits a sine squared relationship as a function of the applied electric field. The optical power of the two polarization directions of interest are out of phase with each other by $\pi/2$. With an analyzer oriented at $-\pi/4$ with respect to the x-y plane, the transmitted optical intensity with zero applied electric field is nominally zero. When a 1/4 wave plate is added to the optical configuration, the transmitted optical intensity with zero applied electric field moves to the inflection point of the sine squared relationship between the transmitted intensity and the applied electric field. This results in maximum sensor linearity, and it is referred to as optical biasing.

For the optical system defined in Figure 1, the output intensity can be written for the $+\pi/4$ and $-\pi/4$ final polarizer directions as follows:

$$I_1 = I_o \sin^2(\Gamma(E)/2 - \pi/4) \quad (1)$$

$$I_2 = I_o \sin^2(\Gamma(E)/2 + \pi/4) \quad (2)$$

where:

I_o = input optical power
$\Gamma(E)$= induced birefringence due to the applied electric fields

Subsequently, the detected optical power is a function of the applied electric field in a sensor which utilizes an electro-optic crystal as a sensing element.

The majority of the work that was performed during the Phase I research effort was with $Bi_4(GeO_4)_3$ (BGO) electro-optic crystals. This is because it was apparent very early in the experimental effort that the BGO crystals were superior to the KDP crystals which were also investigated (see section 2.2). With BGO crystals two directions of applied electric fields are of interest. Figure 2 shows the orientation of the fast and slow axes for the case of electric fields applied along the <110> and <001> crystal directions. The fact that the principal axes for the index of refraction are oriented at $\pi/4$ with respect to each other for the electric fields applied in these two directions, allows electric field sensitivity only along the <110> or <001> crystal directions with the proper orientation of the input light polarizations. For example, if the incident light is polarized at $\pi/4$ with respect to the <001> crystal direction, an induced birefringence will occur only for applied electric fields in the <001> crystal direction. Similarly, by polarizing the incident beam along the <001> or <110> direction birefringence is induced occurring only for electric fields applied in the <110> crystal direction.

This characteristic of BGO and other $\bar{4}3m$ and 23 electro-optic crystals allows for the possibility of developing an electric field sensor with uni-axial electric field sensitivity. Also, by incorporating two optical axes in a single electro-optic crystal, two independent electric field sensors with orthogonal directional sensitivities are created. Figure 3 shows a schematic of a single crystal sensor which incorporates two optical axes and the polarizer and analyzer orientations.

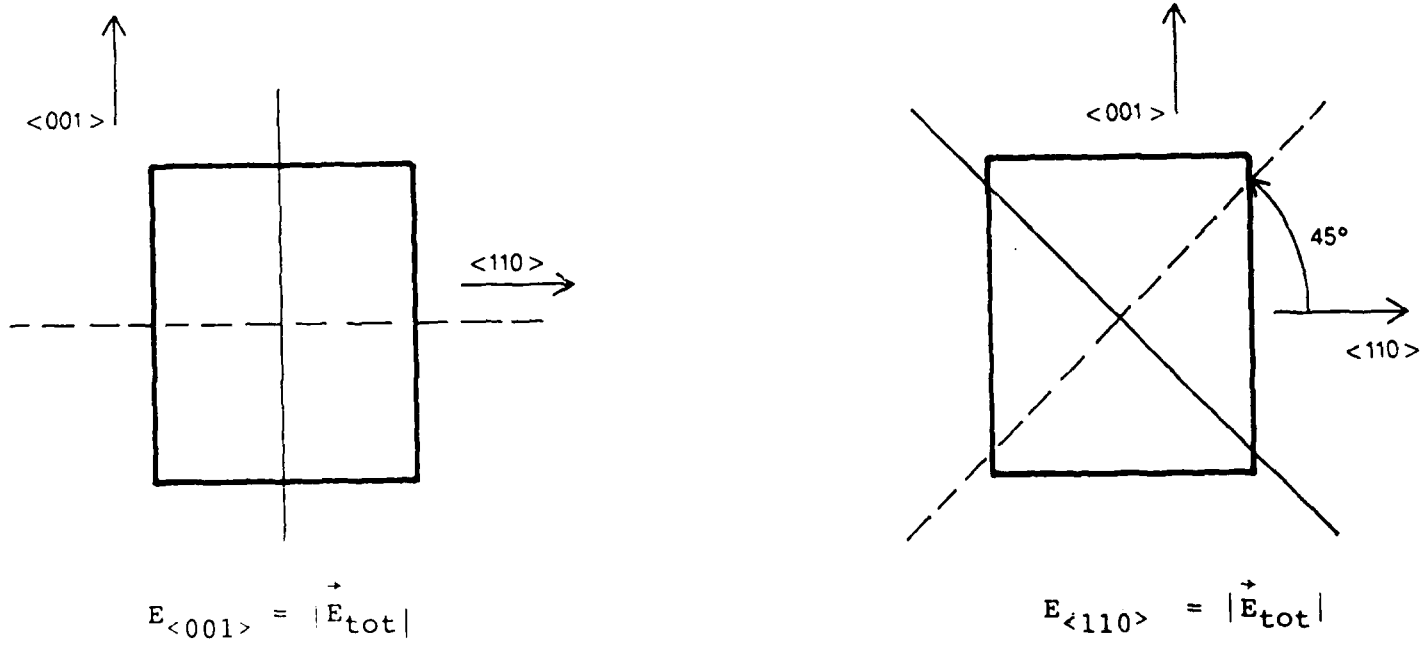

FIGURE 2. Orientation of fast and slow axes in BGO crystals for electic fields applied along the <001> and the <110> crystal directions.

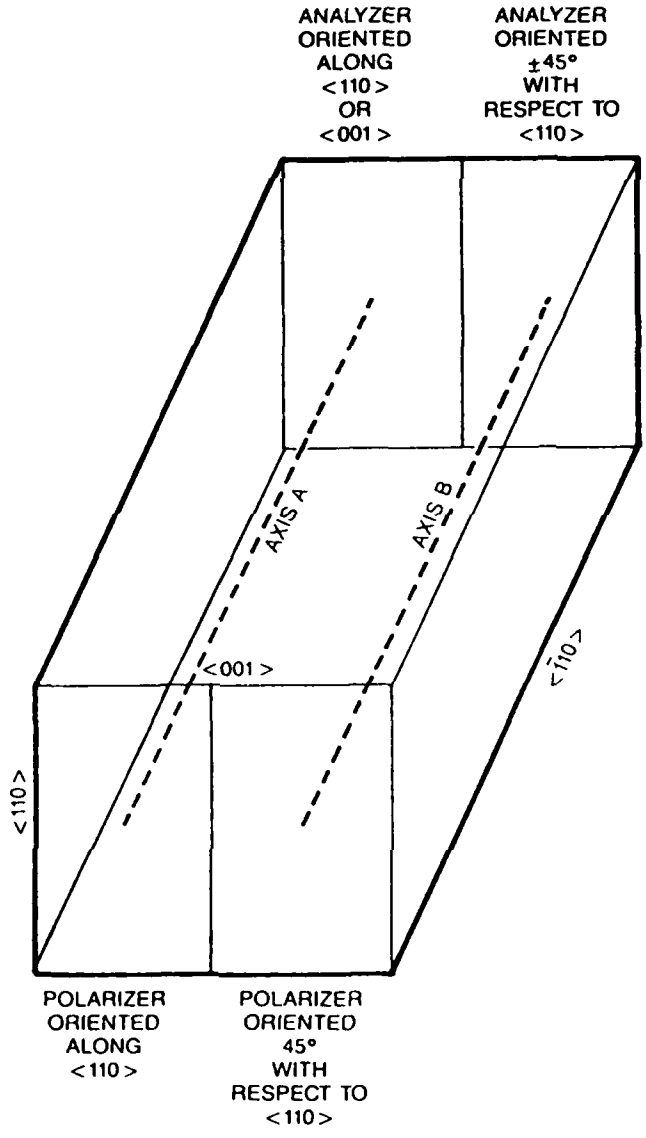

Figure 3. Two optical axes in one crystal
By incorporating two optical axes (A and B) and polarizing axes as shown in a single crystal, independent sensors with orthogonal directional sensitivities are realized.

By incorporating two electro-optic crystals mounted orthogonally in a single head, a fiber optic electric field sensor with 3 axis electric field sensitivity is created. This allows for the measurement of both electric field strength and direction. Figure 4 shows the orientations of two BGO crystals which would afford three-dimensional electric field measurement capabilities. In this case, the component of the electric field in the x direction is measured by both crystals.

In BGO electro-optic crystals, the induced birefringence as a function of the applied electric fields in the <001> and <110> directions is found to be:

$$\Gamma(E) = \frac{2\pi}{\lambda} n_o^3 r_{41} E L \qquad (3)$$

for fields applied along the <110> direction and

$$\Gamma(E) = \frac{\pi}{\lambda} n_o^3 r_{41} E L \qquad (4)$$

for fields applied along the <001> direction.

Where:

λ = the wavelength of the optical source
n_o = crystal index of refraction
r_{41} = electro-optic coefficient
L = crystal length (parallel to $\langle\bar{1}10\rangle$ in $Bi_4(GeO_4)_3$)
E = is the applied electric field.

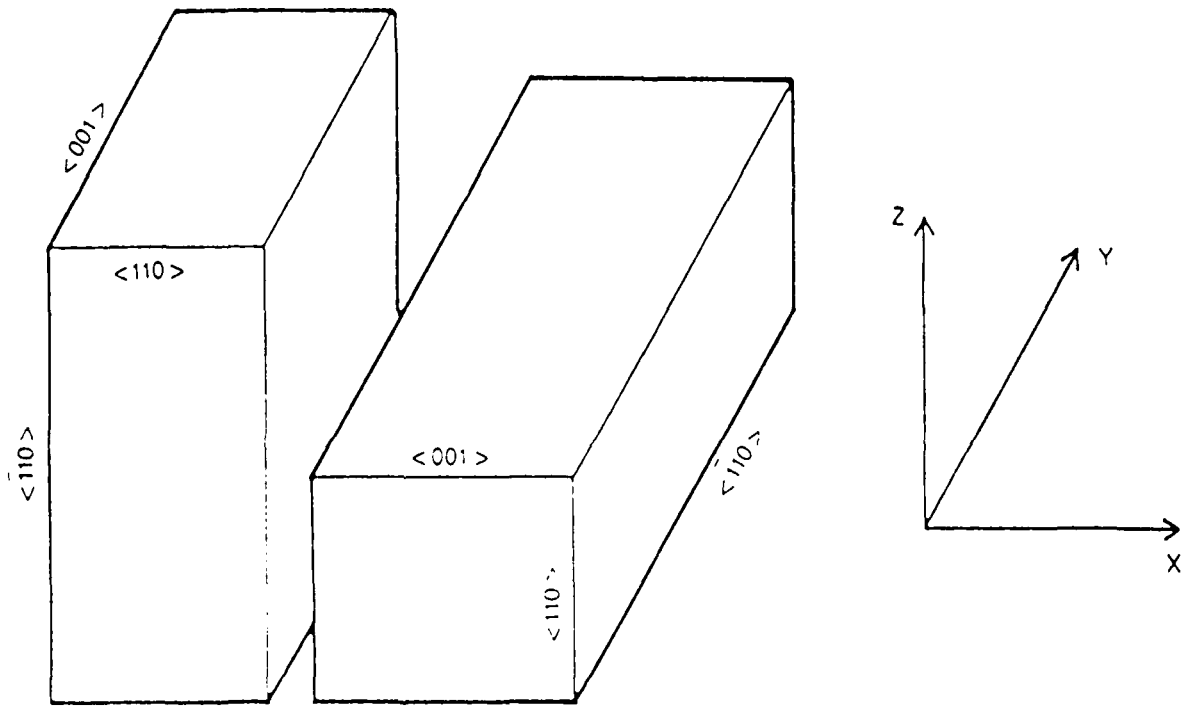

Figure 4. Crystal orientations for a 3-axis electric field sensor utilizing BGO electro-optic crystal (X direction is redundant)

GEO-CENTERS, INC.

The formal derivation of this result is given in Section 3.2 of this report.

Equations (3) and (4) show that the electric field induced birefringence is directly proportional to the crystal length. The longer the crystal along the $\langle \bar{1}10 \rangle$ crystal direction, the greater the induced birefringence for a given applied electric field. The Phase I research effort experimentally determined the effect of crystal length on the electric field induced birefringence. This is a quantitative measure of how the crystal length affects the linear sensing range and the electric field sensitivity of a fiber optic electric field sensor.

Because the electro-optic effect is in principle very fast (it depends on the movement of electrons in a material), it will be assumed that the A.C. bandwidth will be limited by the transit time of light through the crystal because the electric field should be uniform during this time.

The transit time as a function of crystal length is found to be:

$$t = \frac{Ln_o}{C} \qquad (5)$$

where:

C = speed of light
t = time of transit
L = crystal length
n_o = crystal index of refraction

The transit time and, therefore, the A.C. measurement bandwidth capability of a fiber optic electric field sensor is directly proportional to the length of the electro-optic crystal employed. The shorter the crystal, the higher the A.C. measurement bandwidth capability in a fiber optic electric field sensor. The Phase I research effort investigated the effect of crystal length on sensor A.C. measurement bandwidth capability.

The Equations (1) and (2) can be re-expressed in the following form:

$$I_1 = I_o/2 - I_o \sin \Gamma(E)/2 \cos \Gamma(E)/2 \quad (6)$$

$$I_2 = I_o/2 + I_o \sin \Gamma(E)/2 \cos \Gamma(E)/2 \quad (7)$$

This allows the sum and difference of these two equations to be written as follows:

$$I_{sum} = I_1 + I_2 = I_o \quad (8)$$

$$I_{diff} = I_2 - I_1 = 2\ I_o \sin \Gamma(E)/2 \cos \Gamma(E)/2 \quad (9)$$

The sum-difference output becomes:

$$\frac{I_{diff}}{I_{sum}} = 2 \sin \Gamma(E)/2 \cos \Gamma(E)/2 \quad (10)$$

Equation (10) shows that the sum-difference output is intensity invariant, making this the preferred detection scheme for operating a fiber optic electric field sensor in environments where fiber darkening might occur, or where input light intensity variations are anticipated. This output detection scheme would

be useful for an electric field sensor for NEMP research. It is also useful for an electric field sensor for the measurement of very small electric fields. This is because intensity noise associated with the optical source is eliminated with this output detection scheme.

2.2 Comparison of Electro-Optic Crystals for Electric Field Sensors

The electro-optic effect has been utilized in both bulk optical and fiber optic sensors. The majority of published work has been geared to the development of electric field sensors for the power transmission and generation industries and the development of fiber optic voltage sensors. Only one paper utilizes a $Bi_4(GeO_4)_3$ electro-optic crystal(1). This work did not utilize the capability of a single BGO crystal to operate as two independent sensors with orthogonal directional sensitivity. In fact, all electro-optic crystals with 23 or $\bar{4}3m$ point group symmetries have this capability. Although other optical sensors have been developed with crystals having these point group symmetries, this is the first reported time that the capability has been utilized in an optical sensor.(2,3,4) It is felt that this result is unique enough to mandate beginning the motions in the filing of a patent.

Optical electric field and voltage sensors have been developed using $Bi_{12}GeO_{20}$(4), $Bi_{12}SiO_{20}$(2,3), KDP(5), ADA(5), ADP(6) amd KD*P(7), and $Bi_4(GeO_4)_3$(1), electro-optic crystals. By the proper choice of crystal geometry, each of these crystals has the capability of being utilized as the sensing element in a fiber optic electric field sensor. However, for the reasons discussed below, $Bi_4(GeO_4)_3$ is the optimum crystal for developing an electric field sensor for lightning research.

An electro-optic crystal which would be useful as a sensing element in a fiber optic electric field sensor for lightning research must have the following physical characteristics:

1) Ruggedness
2) Insolubility in water
3) Insolubility in grease removing solvents
4) Small electric permeability
5) Large electrical resistance
6) No pyro-electricity
7) No optical activity
8) No natural birefringence

KDP and its related isomorphs (ADA, ADP, KD*P) exhibit large electro-optic effects. These crystals are, however, both hygroscopic and water soluble. Subsequently, in order to prevent deterioration of the crystals, hermetic sealing is required. They are of crystal point group $\bar{4}2m$, which results in a very temperature sensitive electro-optic r_{63} coefficient. KDP's low thermal conductivity in conjunction with its large thermal coefficient of expansion make these crystals susceptible to fracture during routine handling. In addition, KDP and its related isomorphs have natural birefringence which results in temperature sensitivity in an electric field sensor. These crystal properties make KDP and its related isomorphs difficult to utilize in a fiber optic sensor.

$Bi_{12}SiO_{20}$ and $Bi_{12}GeO_{20}$ have 23 crystal point group symetries,and consequently, they exhibit optical activity. This quality makes their use more difficult in a fiber optic electric field sensor. The optical activity results in a polarization rotation occurring during an optical beam's transit through a

crystal. The fabrication of an optical sensor becomes significantly more difficult because of this polarization rotation.

$Bi_4(GeO_4)_3$ has all of the qualities listed earlier for good candidate materials for the development of a fiber optic electric field sensor. During the Phase I research effort, these crystals proved to be exceptionally rugged, not soluble in the typical solvents used for cleaning optical components, and most importantly, these crystals can survive a direct electrical discharge. In addition, these crystals can be easily cut to a geometry which makes their linear sensing range and A.C. measurement bandwidth capabilities applicable to the measurement requirements of the lightning research field.

3.0 Phase I Results

3.1 Summary

GEO-CENTERS, INC. Phase I research goal was to investigate the feasibility of developing a fiber optic electric field sensor based on the electro-optic effect for lightning research applications. $Bi_4(GeO_4)_3$, (BGO), and $KH_3(PO_4)$ (KDP) were cited by GEO-CENTERS, INC. as electro-optic crystals whose electrical and optical properties make them good electro-optic crystals for developing an electric field sensor. The theoretical calculations which were used as the basis for the selection of BGO and KDP crystal geometries are presented. Experimental results from tests performed at GEO-CENTERS, INC. Boston Laboratory facility as well as at AFWAL/FIESL facility in Dayton, Ohio show the feasibility of utilizing this technology for the measurement of both D.C. and A.C. electric fields. These results are used to substantiate the conclusion that BGO is not only the best available electro-optic crystal for this application, but that a sensor using this material promises to be useful for a wide range of electric field measurement applications.

3.2 Theory

The theory section shows the derivation of the induced birefringence with applied electric field for BGO and KDP cyrstals. The theoretical basis for the unique capability of a single BGO crystal to operate as two independent electric field sensors with orthogonal directional sensitivities is derived. The theory also shows that crystals with point group symmetry $\bar{4}3m$, such as BGO, are clearly superior for use in electric field sensors, when

compared to crystals of point group symmetry $\bar{4}2m$ such as KDP. The theoretical results are summarized in Section 2.1 of this report.

The fiber optic electric field sensor is based on induced birefringence in electro-optic crystals resulting from the electro-optic effect. The electro-optic effect is a well understood phenomenon in which the indices of refraction of an electro-optic crystal change when an electric field is applied. The resulting indices of refraction can be described by the index ellipse or indicatrix represented by the following equation:

$$\sum_{ijk} (1/n^2_{ij} + r_{ijk} E_k) x_i x_j = 1 \qquad (11)$$

where:

r_{ijk} = the electro-optic coefficients which are specific to a given electro-optic crystal.

x_i, x_j = the polarization directions of the light propagating in the crystal (perpendicular to the direction of light propagation).

n_{ij} = the index of refraction along a given crystal direction (only valid for $i = j$).

E_k = the electric field applied in the k direction.

Equation (11) is the equation of an ellipsoid whose ellipticity changes as a function of applied electric field. For light propagating along a given crystal direction, the eigenvalues of Equation (11) are evaluated on the plane perpendicular to the direction of light propagation in order to determine the indices of refraction for the two normal modes of propagation. If these

two eigenvalues differ, then the speed of light polarized along one eigenvector will be different than the speed of light polarized in the orthogonal direction, and the relative phase difference between these polarizations will change during the transit of the crystal. The induced birefringence with applied electric field can be calculated from this change in phase.

The induced birefringence is found to be:

$$\Gamma_{in} = \Gamma_{tot} - \Gamma_{nat} = L[(k_i - k_j) - (k_{oi} - k_{oj})] \qquad (12)$$

where:

Γ_{in} = electrically induced birefringence
Γ_{nat} = natural birefringence
Γ_{tot} = total birefringence
L = crystal length
k_{oi}, k_{oj} = the wave number of the normal modes of propagation
k_i, k_j = the wave number of the normal modes of propagation with applied field

substituting, $k = \frac{2\pi n}{\lambda}$ into equation (12):

$$\Gamma_{in} = \frac{2\pi L}{\lambda}[(n_i - n_j) - (n_{oi} - n_{oj})] = \frac{2\pi}{\lambda}(\Delta n_i - \Delta n_j) \qquad (13)$$

where:

n_{oi}, n_{oj} = indices of refraction of the normal modes of propagation
n_i, n_j = indices of refraction of the normal modes of propagation with applied field
λ = wavelength of incident light

Δn_i is the change in index of refraction in the i direction with applied electric field; using:

$$\frac{\partial}{\partial n}\left(\frac{1}{n_i^2}\right) = \frac{-2}{n_{oi}^3}\, dn_i \tag{14}$$

and approximating that dn = Δ n we find:

$$\Delta n_i = \frac{-n_{oi}^3}{2}\left(\Delta\frac{1}{n_i^2}\right) \tag{15}$$

substituting equation (15) into equation (13):

$$\Gamma_{in} = \frac{\pi L}{\lambda}\left[n_{oi}^3\left(\Delta\left(\frac{1}{n_i^2}\right)\right) - n_{oj}^3\left(\Delta\left(\frac{1}{n_j^2}\right)\right)\right] \tag{16}$$

The n_i and n_j terms are often dependent on the electro-optic coefficients r_{ijk}. Relationships between these coefficients are determined by a crystal's lattice type and point group symmetry. For instance, all cubic $\bar{4}3m$ lattices have an r_{ijk} matrix of the form:

where a contracted notation has been used.

$$\begin{bmatrix} 0 & 0 & 0 \\ 0 & 0 & 0 \\ 0 & 0 & 0 \\ r_{41} & 0 & 0 \\ 0 & r_{52} & 0 \\ 0 & 0 & r_{63} \end{bmatrix}$$

i,j ——> m
1,1 ——> 1
2,2 ——> 2
3,3 ——> 3
2,3 ——> 4
1,3 ——> 5
1,2 ——> 6

$$r_{41} = r_{52} = r_{63} \tag{17}$$

Equation (11) can be used to calculate n_i and n_j, and, therefore, Δn_i and Δn_j for the normal modes of the crystal. This is done in order to calculate Γ_{in} in an electro-optic crystal.

Now, to apply this theory to a BGO crystal. This crystal has $\bar{4}3m$ symmetry and has been cut into a rectangle with edges $\langle\bar{1}10\rangle$, $\langle 110\rangle$, and $\langle 001\rangle$ as shown in Figure 5. This crystal orientation has been chosen because it leads to a transverse effect that is both large and simple to test experimentally. The indicatrix for a BGO crystal with $\bar{4}3m$ lattice is found from equations (11) and (17) (using the contracted notation):

$$1 = \frac{1}{n_o^2}(x_1^2 + x_2^2 + x_3^2) + 2\, r_{41}\,(E_1x_2x_3 + E_2x_1x_3 + E_3x_1x_2) \quad (18)$$

where:

$n_o^2 = n_{o1}^2 = n_{o2}^2 = n_{03}^2$ as BGO is an isotropic crystal.

Rotating coordinates $\pi/4$, as shown in Figure 6, about the $\langle 001\rangle$ in equation 18 yields:

$$1 = \frac{1}{n_o^2}(X_1'^2+x_2'^2+x_3'^2) + \frac{2r_{41}}{\sqrt{2}}\,[A_1(E_1'-E_2')(x_1'x_3'-x_2'x_3') +$$

$$A_2\,(E_1'+E_2')(x_1'x_3'+x_2'x_3')] + r_{41}\,E_3'\,(x_1'^2-x_2'^2) \quad (19)$$

where:

$$A_1 = \frac{E_1}{|\vec{E}_{tot}|} \qquad x_1 = \frac{1}{\sqrt{2}}(x_1'-x_2')$$

GEO-CENTERS, INC.

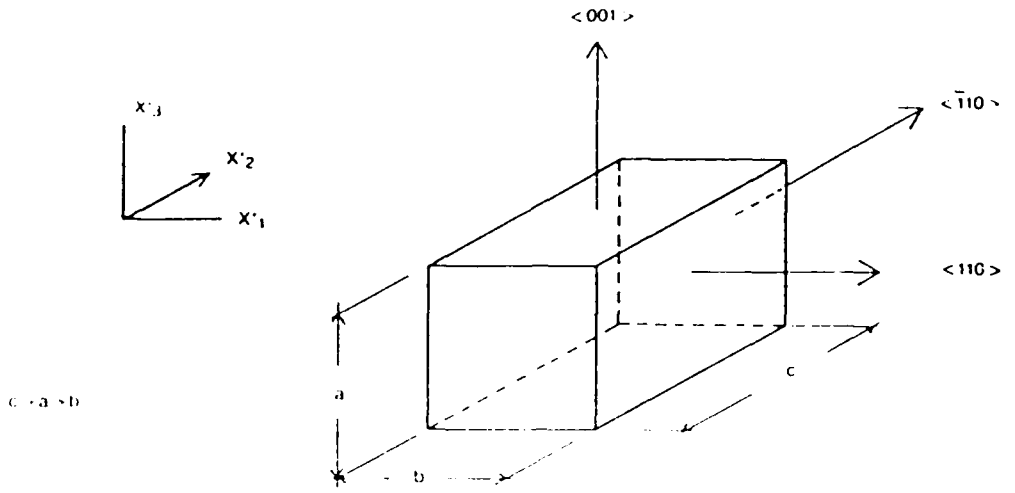

ORIENTATION OF
BGO CRYSTAL

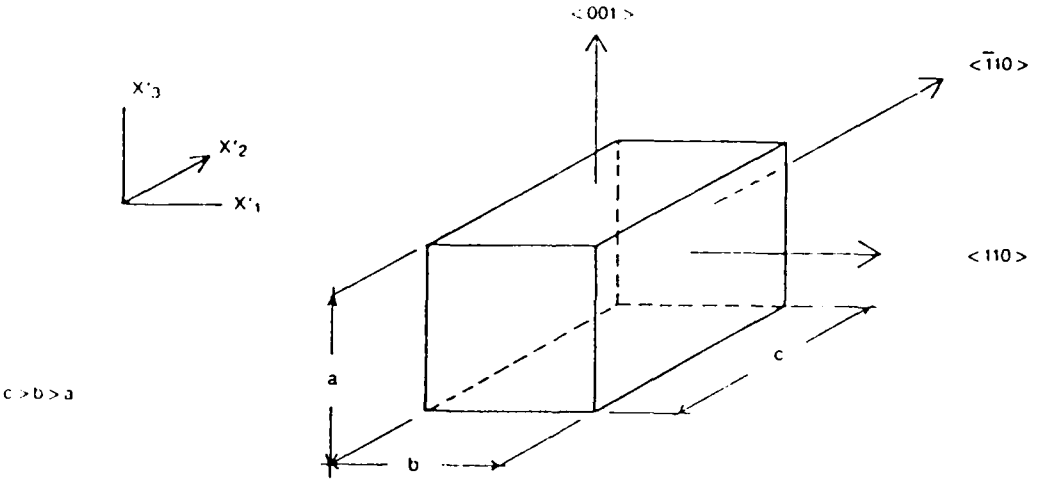

KDP
CRYSTAL ORIENTATION

Figure 5. Crystal orientations.

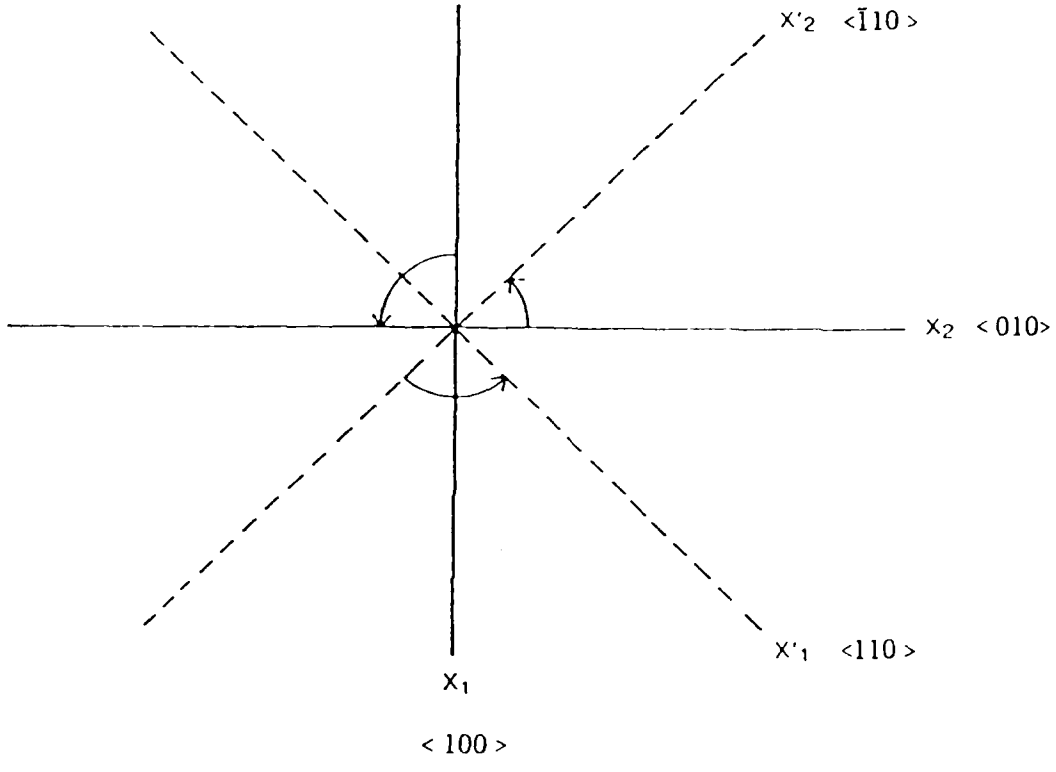

Figure 6. Axes rotation
Rotate axes $\pi/4$ about the X_3 direction.

$$A_2 = \frac{E_2}{|\vec{E}_{tot}|} \qquad x_2 = \frac{1}{\sqrt{2}}(x_1' + x_2')$$

$$E_3 = E_3' \qquad x_3 = x_3'$$

and the primes indicate the new coordinates' directions.

Since the light is propagating in the $\langle \bar{1}10 \rangle$ direction, no light can be polarized along that direction, which is to say that x_2' is zero. Writing equation (19) in matrix form and eliminating the x_2' terms yields:

$$0 = \begin{vmatrix} \frac{1}{n_o^2} + r_{41} E_3' & \frac{r_{41}}{\sqrt{2}} [A_1(E_1' + E_2') + A_2(E_1' - E_2')] \\ \frac{r_{41}}{\sqrt{2}} [A_1(E_1' + E_2') + A_2(E_1' - E_2')] & \frac{1}{n_o^2} \end{vmatrix} \quad (20)$$

diagonalizing the above matrix to determine the eigenvalues, γ:

$$\gamma = 2a + \sqrt{2}M E_3' \pm [(2a + \sqrt{2}M E_3')^2 - 4(a^2 + 2\sqrt{2}M E_3' - M(A_1 \varepsilon_+ + A_2 \varepsilon_-))]^{1/2} \quad (21)$$

where:

$$a = \frac{1}{n^2}$$

$$M = \frac{r_{41}}{\sqrt{2}}$$

$$\varepsilon+ = (E_1'+E_2')$$

$$\varepsilon- = (E_1'-E_2')$$

The induced birefringence with applied electric field will now be calculated for electric fields applied along <110>, <001>, and <$\bar{1}$10> crystal directions.

For E applied along <110> (x_1' direction) equations (20) and (21) yield the following eigenvalues:

$$\frac{1}{n^2} = \frac{1}{n_o^2} \pm r_{41} \left|\vec{E}\right| \tag{22}$$

The eignvectors for this case are oriented at + and - $\pi/4$ with respect to the <001> crystal direction. The relative index of refraction change between these two axes is therefore:

$$\Delta\left(\frac{1}{n^2}\right) = \frac{1}{n^2} - \frac{1}{n_o^2} = 2r_{41} \left|\vec{E}\right| \tag{23}$$

substituting equation (13) into equation (16) yields:

$$\Gamma_{in} = \frac{2\pi}{\lambda} n_o^3 r_{41} LE \tag{24}$$

For E applied along <001> (x_3' = x_3 direction) equations (20) and (21) yield the following eigenvalues:

$$\frac{1}{n^2} = \frac{1}{n_o^2} + r_{41} \left|\vec{E}\right| \text{ and } \frac{1}{n^2} = \frac{1}{n_o^2} \tag{25}$$

The eigenvectors for this case are oriented at 90^{o} and 0^{o} with respect to the <001> crystal direction. The relative index of refraction change between these two axes is therefore:

$$\Delta\left(\frac{1}{n^2}\right) = r_{41} \ |\vec{E}| \tag{26}$$

substituting equation (26) into equation (6) yields:

$$\Gamma_{in} = \frac{\pi}{\lambda} n_o^3 \ r_{41} \ LE \tag{27}$$

For E applied along <$\bar{1}$10> direction (x_2' direction) it is found that the index of refraction does not change with applied electric field.

The fact that the principal axes for the index of refraction are oriented at $\pi/4$ with respect to each other in the case of electric fields applied along the <110> and <001> crystal directions, allows through control of the input light polarization, electric field sensitivity, only along <110> or <001> crystal direction. For example, if the incident light is polarized $\pi/4$ to the <001> direction, birefringence will be induced by electric fields in the E_3' direction only. Similarly polarizing the incident beam along the <001> or <110> direction means that fields in the E_1' direction only will induce birefringence in the electro-optic crystal. This is shown schematically in Figure 7. Hence, each component of an applied E-field can be looked at individually. This allows for the development of an electric field sensor which has uniaxial sensitivity. Also, by incorporating two optical axes in a single electro-optic crystal, two

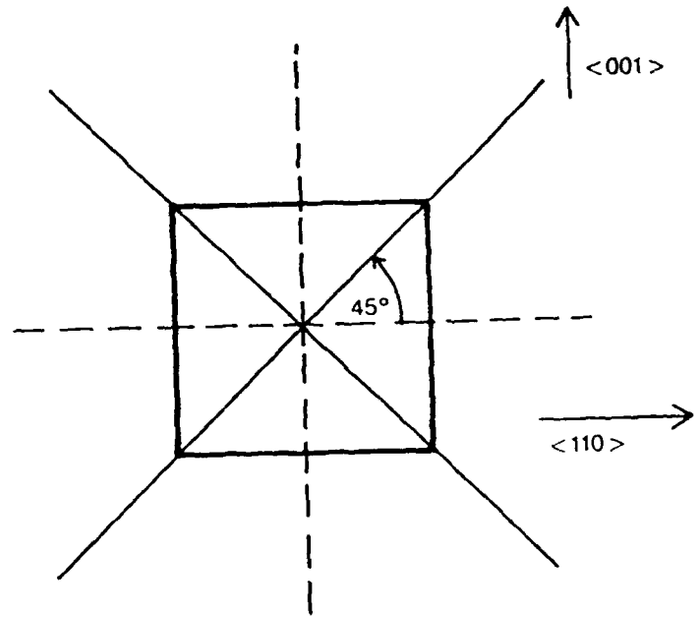

FAST AND SLOW AXES FOR E IN <110> DIRECTION

FAST AND SLOW AXES FOR E IN <001> DIRECTION

Figure 7. Axes orientation with applied electric fields
When light is polarized $\pi/4$ from the <001> axis it is not effected by fields along the <110> direction. When light is polarized parallel to or perpendicular to the <001> axis it is not effected by fields in the <001> direction.

electric field sensors with orthogonal directional sensitivity are realized.

An analysis of the electric field induced birefringence in KDP proceeds in a manner similar to the preceeding calculation for BGO. Again, the light is propagating in the $\langle \bar{1}10 \rangle$ direction in order to have a transverse effect; however, the fact that KDP has the $\bar{4}2m$ crystal symmetry results in $r_{41} = r_{52} \neq r_{63}$ and $\frac{1}{n_{o1}^2} = \frac{1}{n_{o2}^2} \neq \frac{1}{n_{o3}^2}$, leads to a much more complicated expression for the electric field induced birefringence, when it is compared to BGO.

The results for KDP indicate that both the eigenvectors and the eigenvalues are dependent on the applied field. The complications that this dependence creates makes the results of these calculations difficult to interpret and require lengthly analysis. As such, these calculations are reserved for Appendix A.

The directional electric field sensitivity shown in BGO does not exist in KDP. Hence, more complicated deconvolution would be required to extract data from a KDP crystal. The dependence of the eigenvectors on the field further complicates the use of KDP in an electric field sensor since the magnitude of a component of incident light along the principle axes changes as the principle axes change direction with the applied field.

The results show that BGO is an ideal choice for the development of a fiber optic electric field sensor based on the electro-optic effect. A sensor developed using BGO would have uni-directional sensitivity. By incorporating two optical axes in a single crystal, two sensors with orthogonal directional sensitivities can be created. This would allow for the development of an electric field sensor which is capable of measuring both electric field strength and direction with only two BGO crystals.

CED CENTERS INC.

The calculations predict that if the light is polarized + 45° from the <001> axis the crystal will be sensitive only to fields in the <001> direction. On the other hand, if the incident light is polarized along either the <001> or <110> direction the crystal will be sensitive to E-fields in the <110> direction only. On the basis of the calculations, rectangular BGO crystals were cut with edges along the $\langle\bar{1}10\rangle$, <110> and <001> directions.

3.3 Experimental Results

GEO-CENTERS, INC.'s experimental effort concentrated on demonstrating the feasibility of utilizing an electro-optic crystal as a sensing element in a fiber optic electric field sensor with measurement capabilities applicable to the lightning research area. This section first describes the instrumentation which was used to make the measurements, and experimental results are then presented which show the electro-optic crystals' response to D.C. electric fields. Results from experiments performed to characterize electro-optic crystals' A.C. electric field sensitivity are given. The results from these experiments show that a fiber optic electric field sensor can be developed using a BGO crystal which has capabilities that make it excellently suited to lightning research applications.

3.3.1 Instrumentation

When linear polarized light travels through a birefringent material, the light becomes elliptically polarized. In order to measure the birefringence an ellipsometer is used. Figure 8 shows the set-up of the breadboard ellipsometer used at GEO-CENTERS, INC. to make measurements of electric field induced birefringence. The ellipsometer consists of an input polarizer, a linear compen-

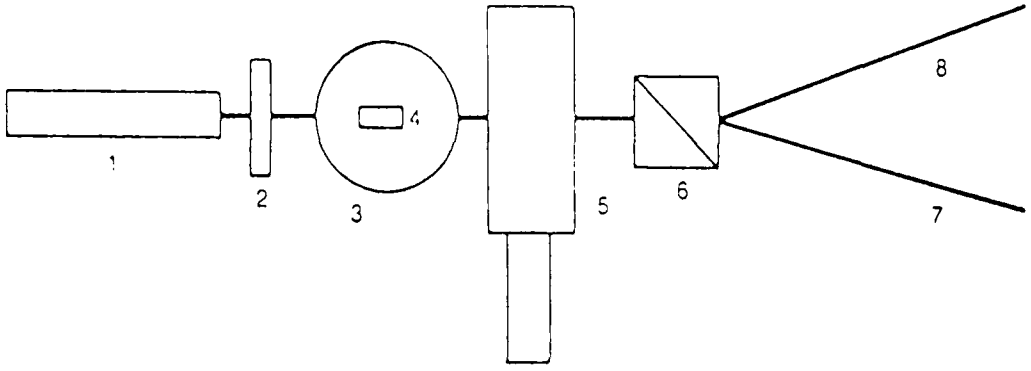

1) HeNe LASER (5 mW)
2) LINEAR POLARIZER
3) TEST PLATES
4) CRYSTAL
5) LINEAR COMPENSATOR
6) WOLLASTON PRISM
7,8) TWO INDEPENDENT LINEAR POLARIZATION STATES

POWER SUPPLY AND DETECTORS CHOSEN FOR SPECIFIC APPLICATION

Figure 8. GEO-CENTERS, INC.'s ellipsometer

sator (a variable wave plate typically used as a 1/4 wave plate), a Wollaston prism (used as an analyzer), and one or two photodetectors used to monitor the light intensity transmitted through the system. Test plates were incorporated into the breadboard ellipsometer to produce electric fields. The test plates are made of copper cladded circuit board and are held apart by either 1 cm or 2 cm PVC spacers.

With the input polarizers and the Wollaston prism aligned at $\pi/4$ with respect to the induced fast and slow axis we find:

$$\frac{I+}{I_o} = T+ = \sin^2\left(\frac{\Gamma(E)}{2} - \frac{\Gamma(LC)}{2} \right) \tag{28}$$

$$\frac{I-}{I_o} = T- = \sin^2\left(\frac{\Gamma(E)}{2} + \frac{\Gamma(LC)}{2} \right) \tag{29}$$

where:

- $I+$ = transmitted intensity along the input polarization direction
- $I-$ = transmitted intensity orthogonal to the input polarization direction
- I_o = total incident intensity
- $T+$ = % transmission along the input polarization direction
- $T-$ = % transmission orthogonal to the input polarization direction
- $\Gamma(E)$ = induced birefringence with applied electric field
- $\Gamma(LC)$ = birefringence due to the linear compensator (adjustable)

In order to make measurements of the induced birefringence, the input polarizer is aligned at $\pi/4$ with respect to the induced fast and slow axes of the electro-optic crystal. For BGO this orientation is at $\pi/4$ with respect to the <001> crystal direction for electric field sensitivity only along the <001> direction, or aligned with the <001> crystal direction for electric field sensitivity only along the <110> crystal direction. The linear compensator is oriented so that its fast and slow axes are aligned with the crystal fast and slow axes. The compensator is adjusted so that the transmitted optical intensity is at the inflection point of the sine squared relationship between birefringence and the transmitted optical intensity as represented in Equations (28) and (29). This provides the maximum sensitivity to electric field induced birefringence and is referred to as optical biasing.

The Wollaston prism orientation is adjusted so that its output polarizations are aligned with, and orthogonal to, the input polarization direction. The photodetectors and amplifiers are chosen to meet a given experimental gain and bandwidth requirement.

The system described above can be used in many different ways to make useful measurements. For instance, if both output polarizations are monitored, the difference in the two transmitted intensities can be measured. If we are nominally biased at the inflection point as given by Equations (28) and (29), the initial difference will be zero. With applied electric field, the difference will become non-zero. The linear compensator can then be adjusted to "null" the difference signal. The change in the birefringence introduced by the linear compensator becomes a direct measurement of the electric field induced birefringence. This technique is best utilized for making measurements of small

changes in birefringence ($\sim 1^{o}$). For many measurement applications, the birefringence changes are large enough to allow the measurements of the electrically induced birefringence to be made by monitoring only the change in transmission of one of the output polarizations. This is the case for the majority of the experiments in the Phase I research effort.

For measuring the induced birefringence in an electro-optic crystal with applied D.C. electric field, the ellipsometer as described above was used (with a single photodetector). A Meret PIN diode was used as the photodetector. The photodetector monitors the intensity change of the output polarization state. The photodetector circuit is shown in Figure 9. For the initial measurements resistor R was 5.1k Ω. In later experiments, R was replaced by a 39 kΩ resistor which affords better measurement sensitivity. In all cases, the PIN circuit output is monitored by a Fluke model 77 handheld multimeter. The power supplies for the test plates were an Ortec -3KV to 3KV power supply and a Sorensen zero to 30KV power supply. This set up is shown schematically in Figure 10.

3.3.2 Response to Applied Electric Fields

3.3.2.1 D.C. Measurements

Experiments were performed to characterize the response of electro-optic crystals to D.C. applied electric fields. These experiments were done in order to investigate the linear sensing range afforded by different electro-optic crystals if incorporated in a fiber optic sensor. The purpose of this investigation is to empirically determine which electro-optic crystals should be incorporated in a sensor for a given measurement requirement.

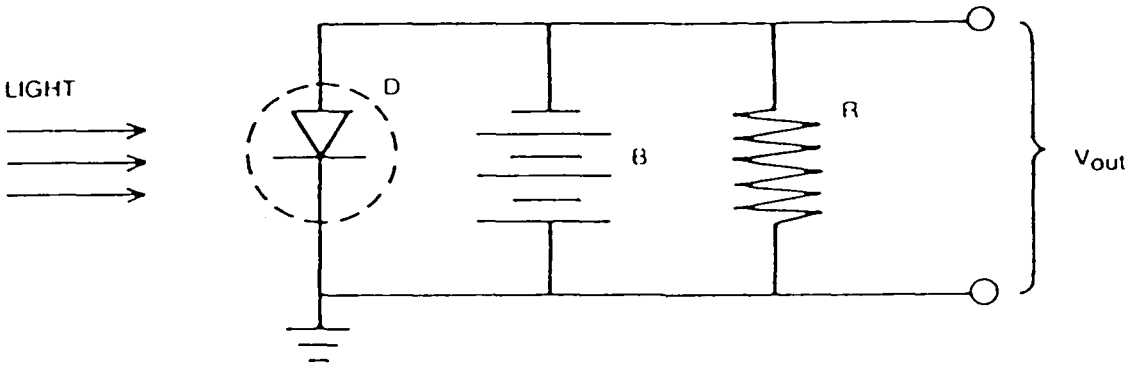

D — MERET PIN DIODE
B — 22½ VOLT BATTERY
R — RESISTOR 5.1KΩ OR 39KΩ

Figure 9. MERET pin diode circuit.

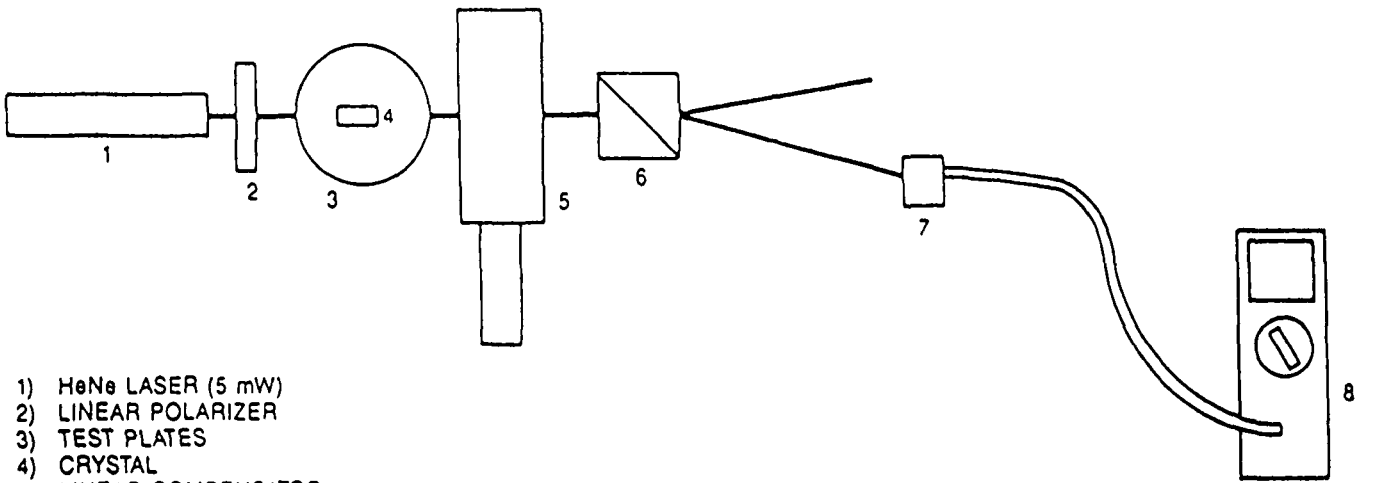

1) HeNe LASER (5 mW)
2) LINEAR POLARIZER
3) TEST PLATES
4) CRYSTAL
5) LINEAR COMPENSATOR
6) WOLLASTON PRISM
7) MERET PIN PHOTODIODE
8) FLUKE MODEL 77 HAND-HELD VOLTMETER

POWER SUPPLY IS EITHER AN ORTEC -3 KV to 3 KV SOURCE
OR A SORENSEN 0 TO 30 KV SOURCE.

Figure 10. Experimental setup for DC measureements.

Both BGO and KDP crystals were utilized in these experiments. The geometries of the crystals are given in Table 1 below:

TABLE 1

Crystal Geometries Incorporated for D.C. Electric Field Tests

BGO			KDP		
$\langle\bar{1}10\rangle$	$\langle 001\rangle$	$\langle 110\rangle$	$\langle\bar{1}10\rangle$	$\langle 001\rangle$	$\langle 110\rangle$
5 mm	3 mm	2 mm	5 mm	2 mm	3 mm
10 mm	6 mm	5 mm	10 mm	5 mm	6 mm
20 mm	6 mm	5 mm	20 mm	5 mm	6 mm

3.3.2.1.1 BGO

Experiments with 5mm BGO crystals established the linearity of the crystals response to applied electric field. Figure 11 shows that in the range $-2.9\text{x}10^5$ V/m to $2.9\text{x}10^5$ V/m the sensor's response to the applied electric field is quite linear. The two data sets on this plot are for the two different output polarization states. As predicted by Equations (28) and (29), the transmission of one polarization increases while the transmission of the other polarization decreases. The data also exhibited no hysteresis indicating that the crystals do not change after being placed in an electric field.

Figure 12 shows the predicted directional sensitivity of the 5 mm BGO crystal. Here, the incident light is polarized at $\pi/4$ with respect to $\langle 001\rangle$ crystal direction. The crystal is only marginally sensitive to fields in the $\langle 110\rangle$ direction. The slight apparent sensitivity to fields in the $\langle 110\rangle$ direction can easily

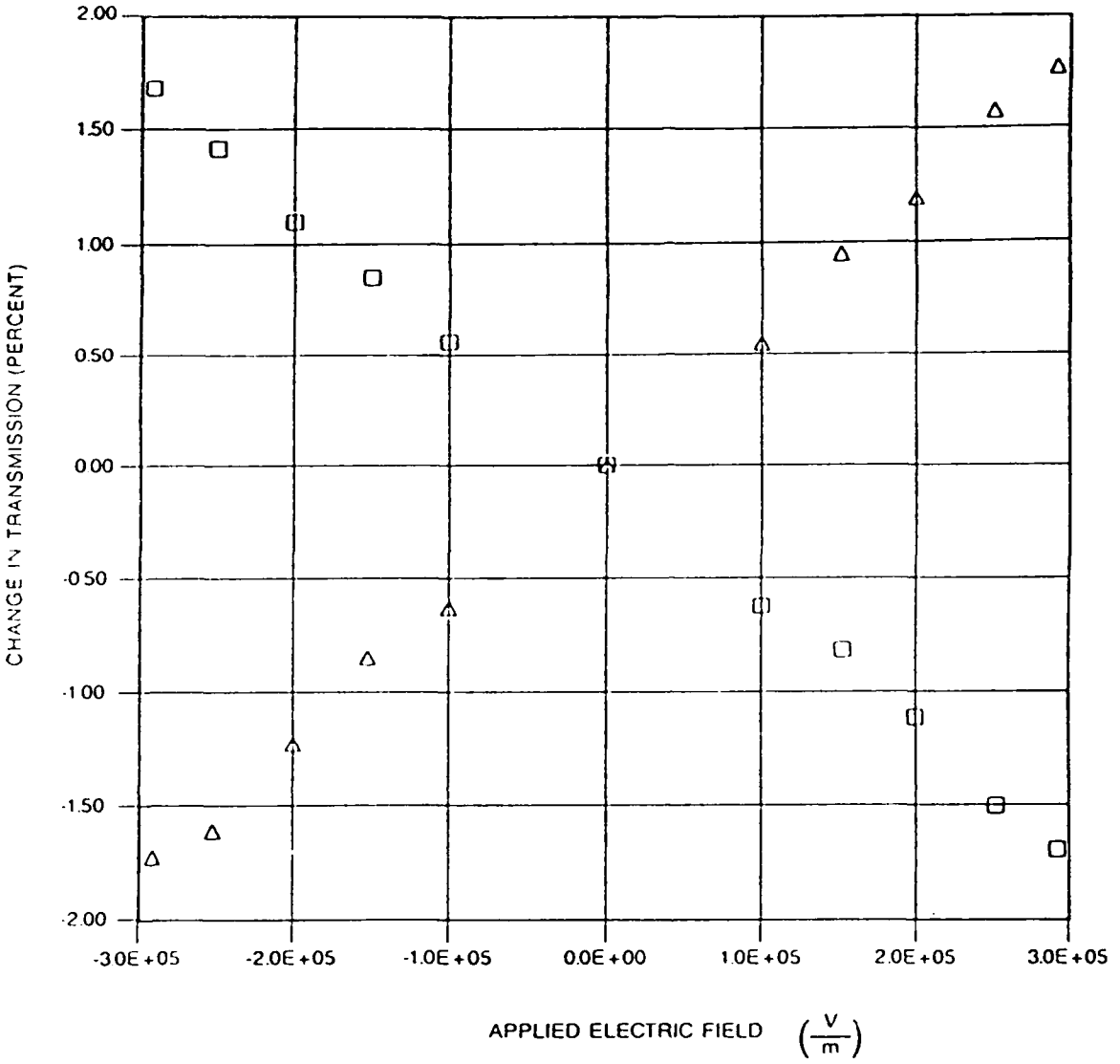

Figure 11. Changes in transmission versus applied field for the two independent polarization states for 5mm BGO.

be accounted for by ellipsometer misalignments and inexact crystal axes orientation. By rotating the linear polarizer $\pi/4$ and rotating the linear compensator $\pi/4$ from vertical, the directional sensitivity of the crystal changed. Now the crystal was very sensitive to fields in the <110> direction and only slightly sensitive to fields in the <001> direction. This situation is shown in Figure 13. The apparent sensitivity of the crystal to fields in the <001> direction can again be accounted for by misalignments.

Equation 16 indicates that the induced birefringence in an electro-optic crystal with applied electric field is dependent on the length of the crystal. The longer the crystal, the larger the induced birefringence for a given applied electric field. This suggests that a longer crystal would more easily detect a small electric field. However, longer crystals might exhibit so much induced birefringence that the response is no longer linear. This non-linearity is caused by the non-linearity of the sine squared relationship between the transmitted optical intensity and the induced birefringence as represented in Equations (28) and (29). Figure 14 compares the responses of the 5mm, 10mm, and 20mm crystals. Note that each crystal exhibits a linear relationship over the entire range of the applied electric field. Figures 15, 16, and 17 show the response of the 5 mm, 10 mm, and 20 mm crystals respectively over a limited range of the applied electric field. These data clearly shows the effect of crystal length on the D.C. measurement capability (linear sensing range), for BGO crystals. A 20mm crystal can more accurately detect a smaller electric field as the signal to noise ratio increases with crystal length.

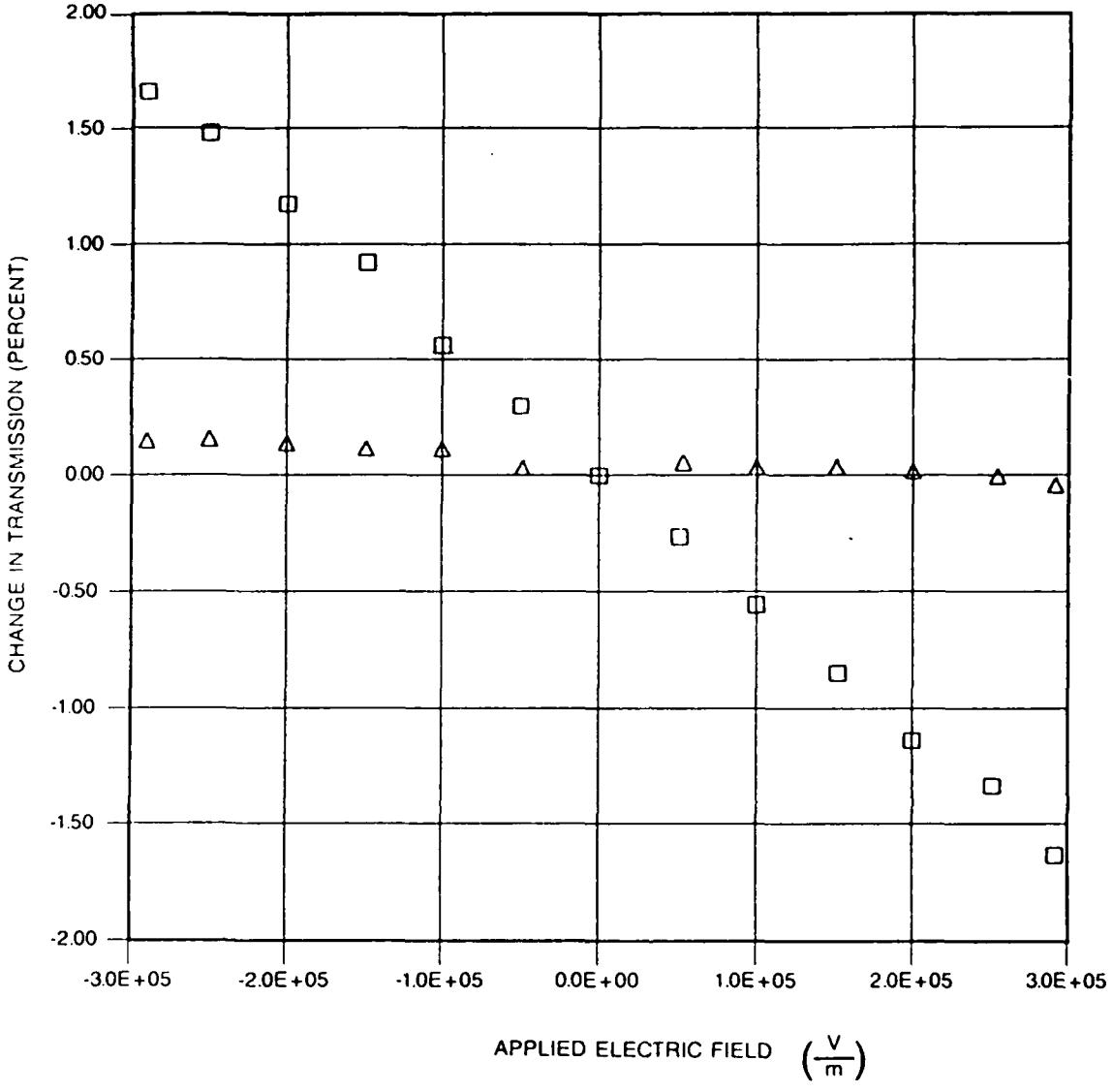

Figure 12. Change in transmission versus applied fields for 5mm BGO crystal.

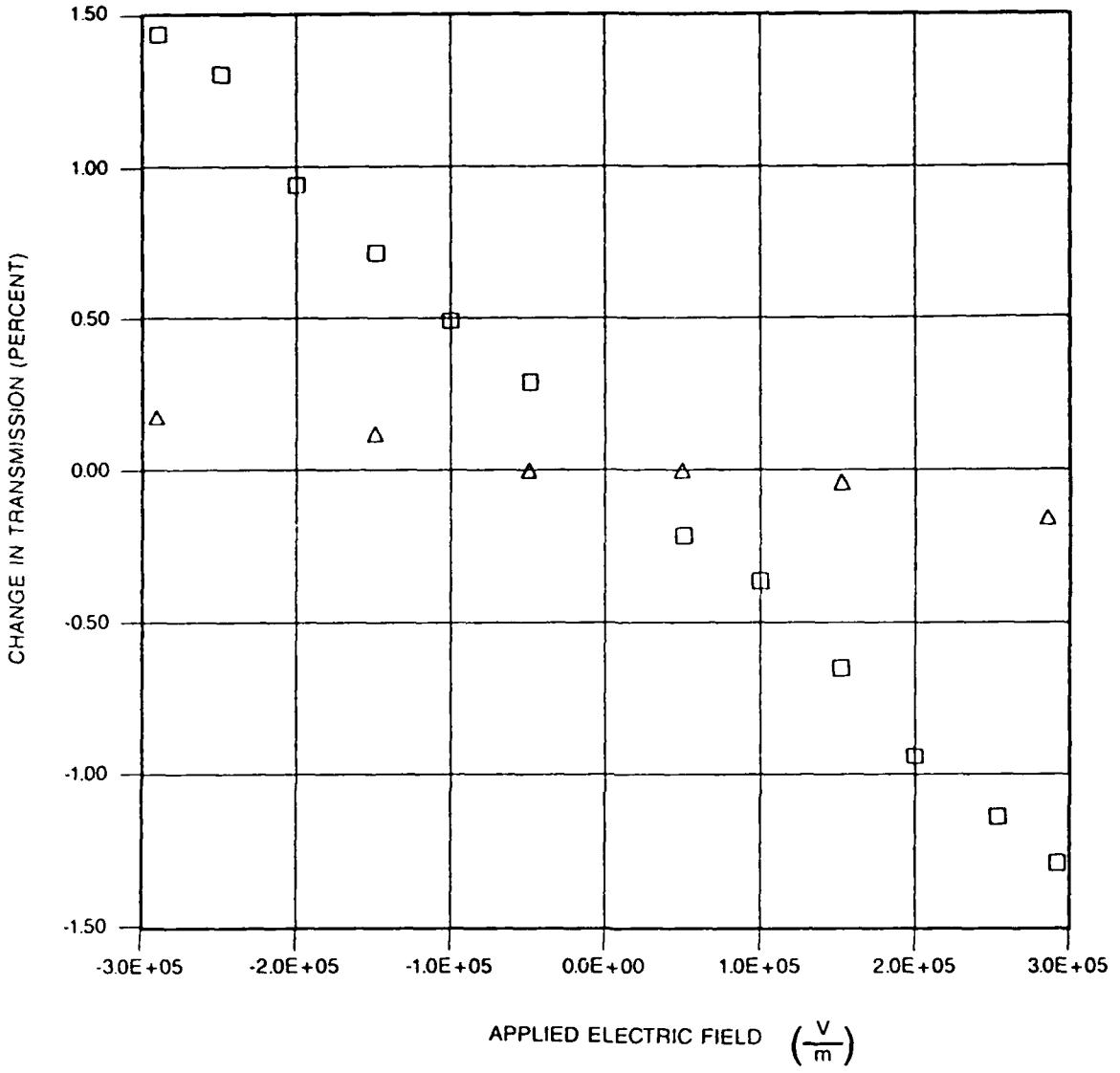

□ FIELD ALONG <110>

△ FIELD ALONG <001>

Figure 13. Change in transmission versus applied field for 5mm BGO crystal.

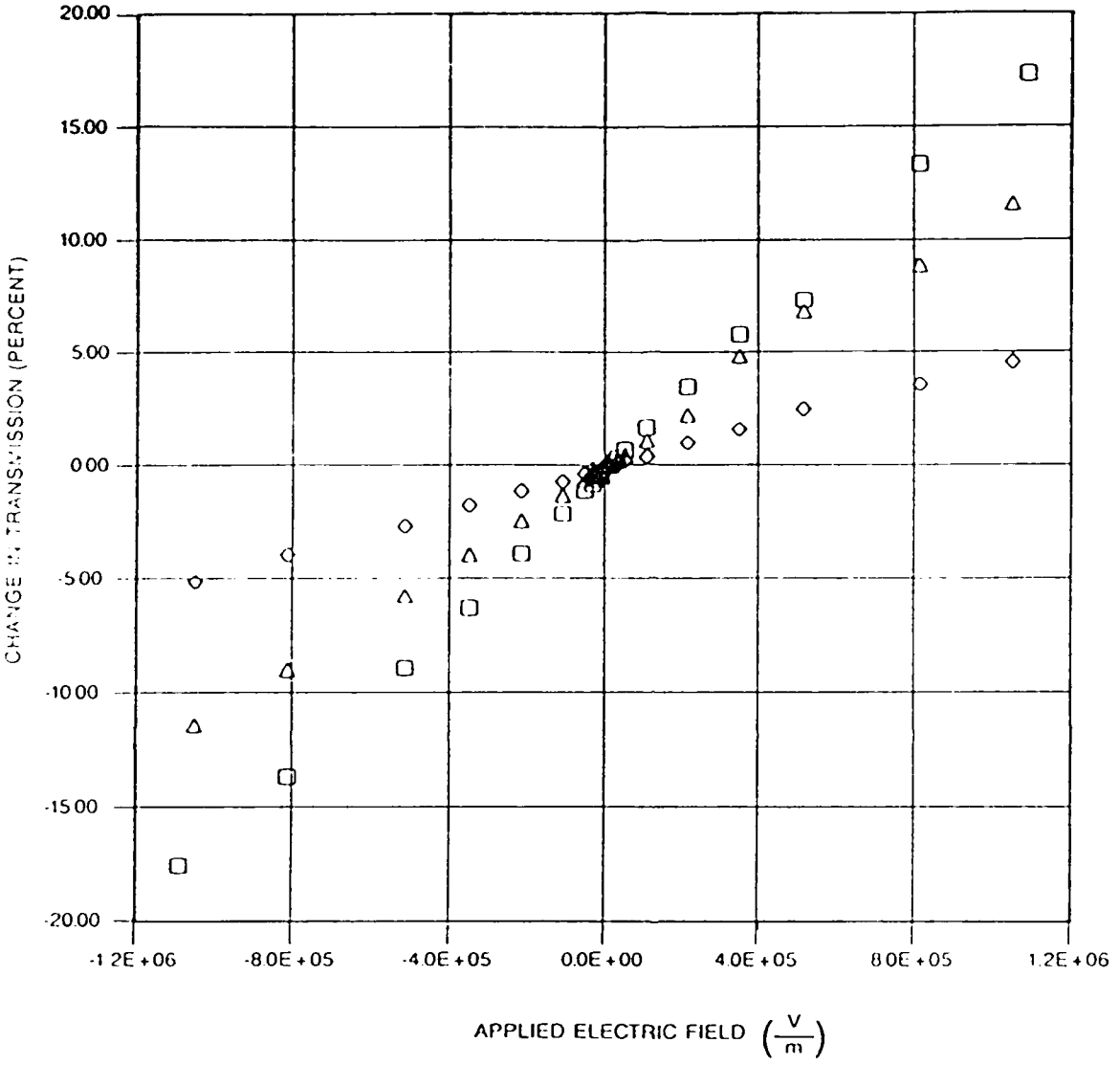

Figure 14. Comparison of transmission change for three different crystal lengths in BGO.

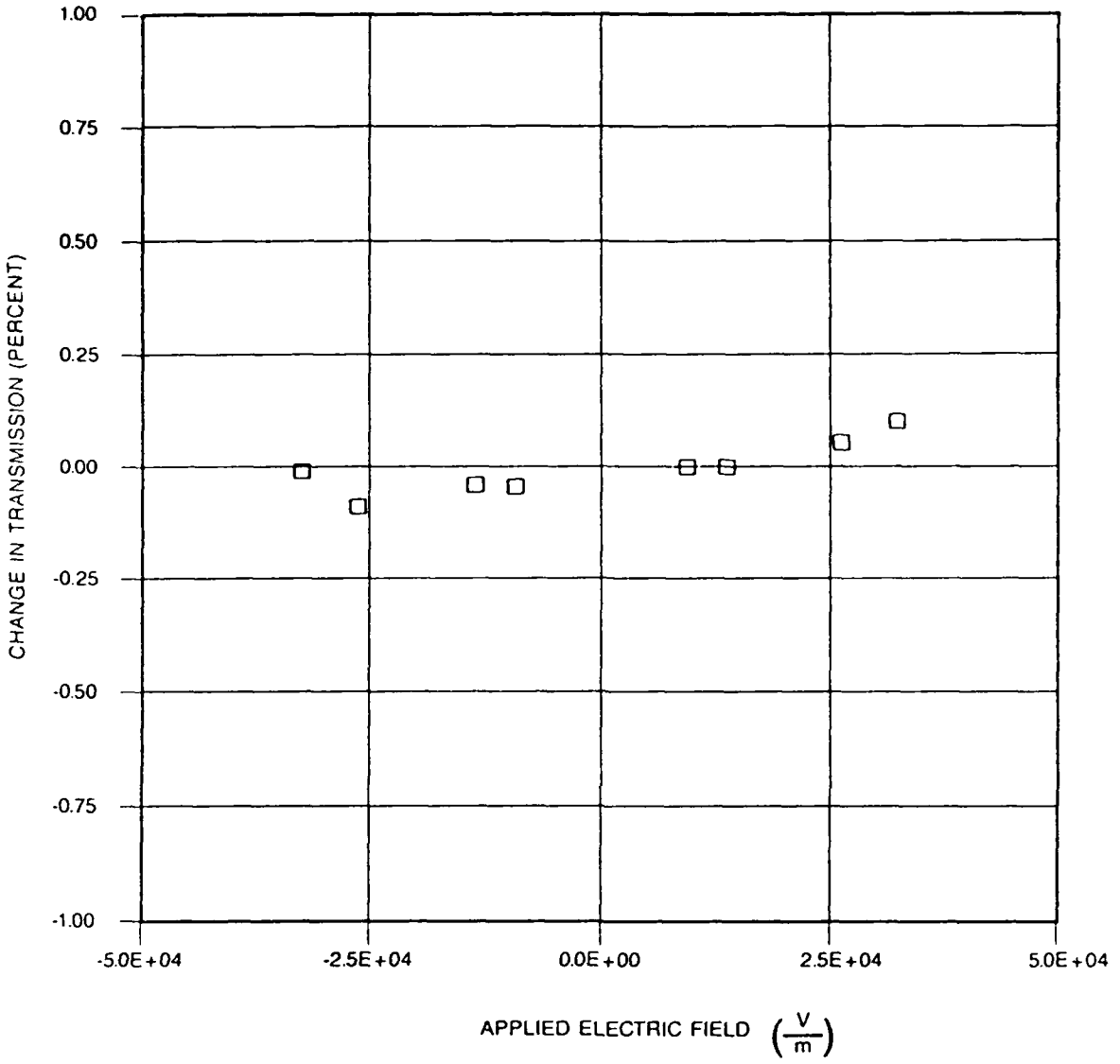

Figure 15. Change in transmission versus applied electric field in BGO.

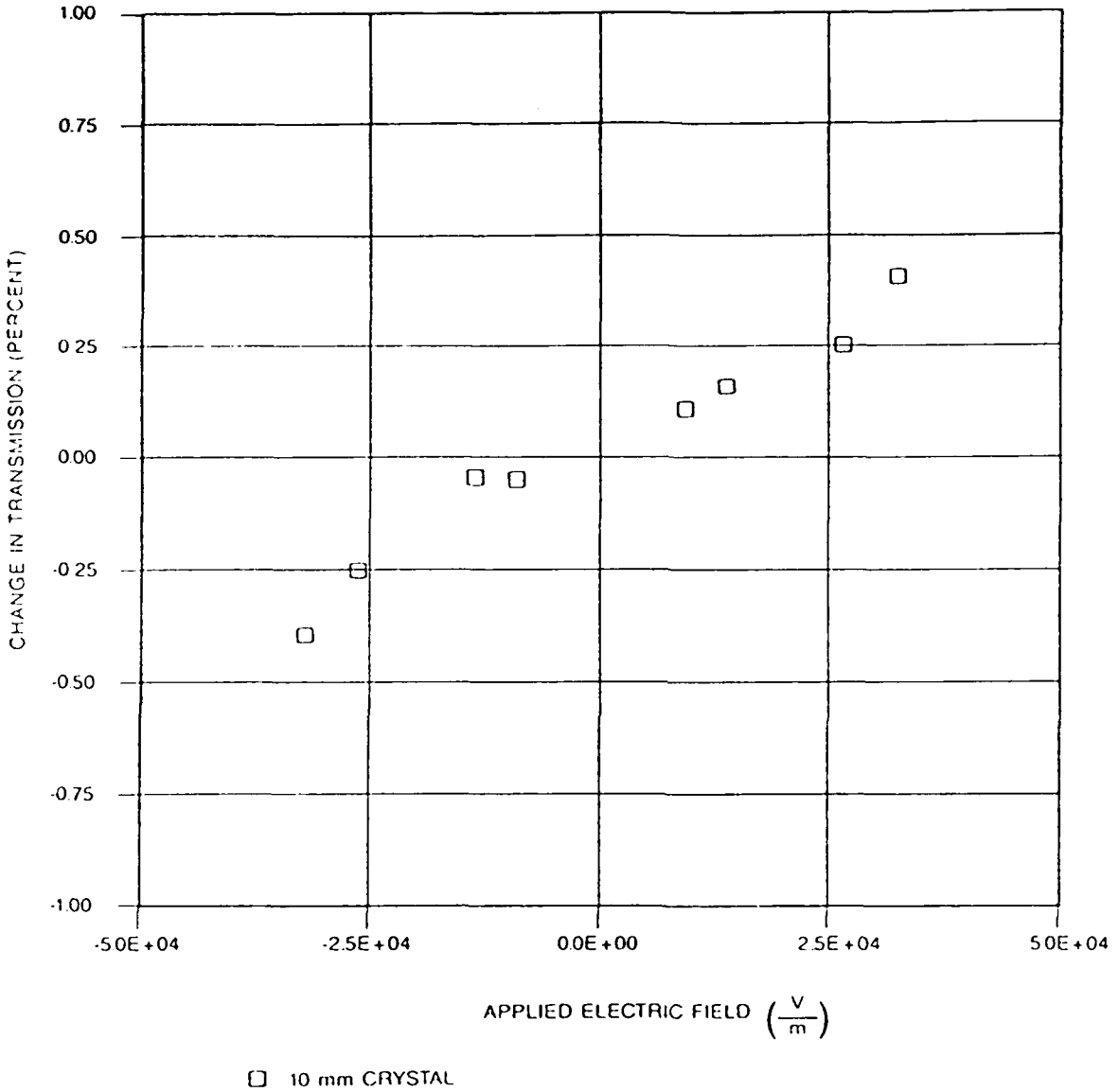

Figure 16. Change in transmission versus applied electric field in BGO.

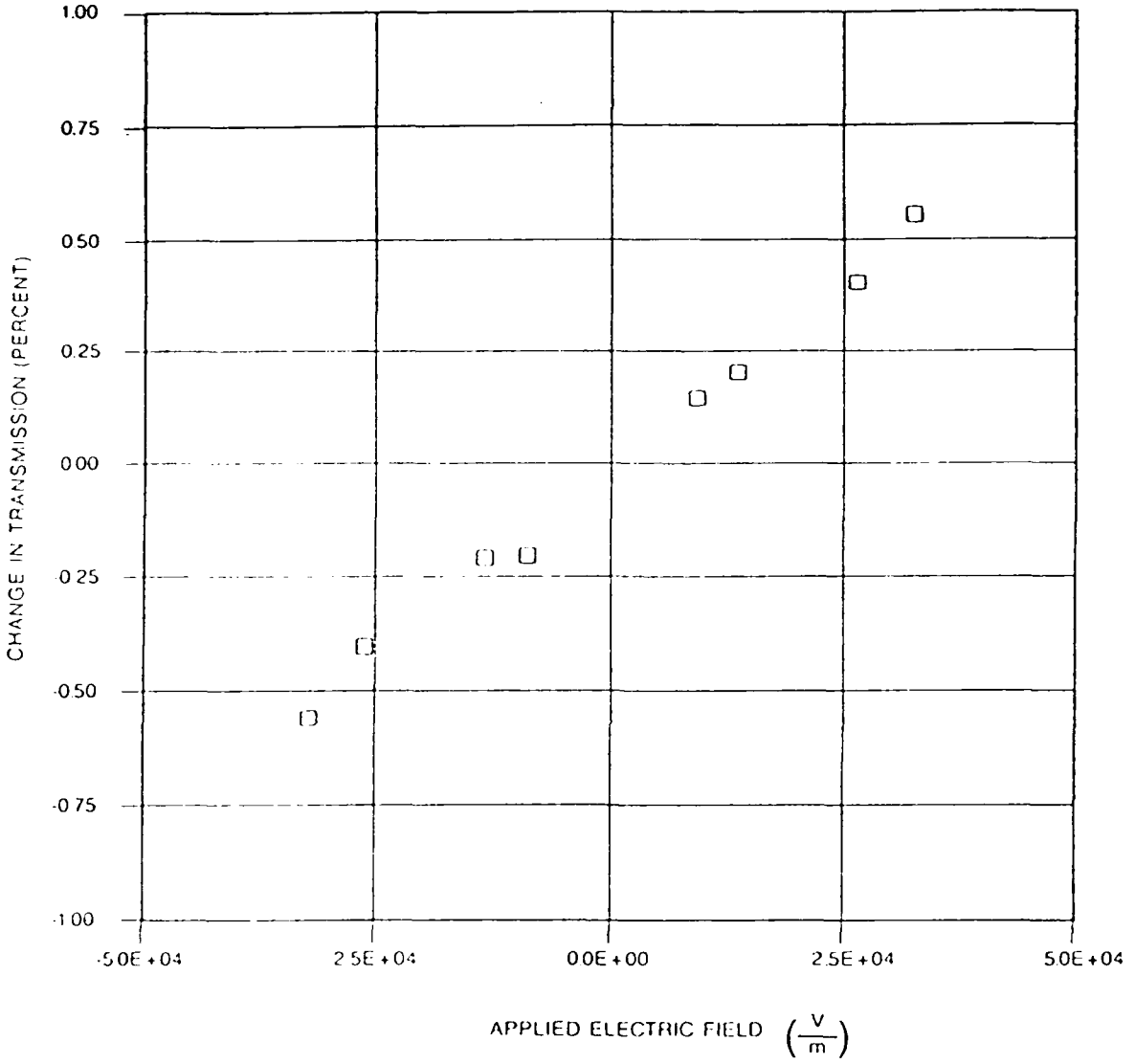

Figure 17. Change in transmission versus applied field in BGO.

3.3.2.1.2 KDP

In contrast, the KDP crystals showed none of the useful characteristics shown by the BGO. Instead, the KDP exhibited an oscillating birefringence with no applied field as shown in Figure 18. This means that the two output polarization do not establish a steady value from which changes could be measured.

The KDP crystal did exhibit large depolarization effects. This means that when the crystal was put into a quickly changing field the birefringence was initially changed significantly but then reduced to the no field level again. Upon turning the field off, the same type of behavior was observed. These depolarization effects occurred too quickly to allow any useful data to be taken on the KDP crystals.

Depolarization effects such as the ones observed with KDP are often caused by some conducting layer that is in contact with the entire surface of the crystal. This layer acts as a charge carrying medium allowing charges to reduce their potential energy. Hence, the external field will be cancelled out as the result of the charge movement (Figure 19).

Since KDP is not a rugged crystal it is not easily cleaned of these layers. In addition, the hygroscopic nature of KDP probably causes the surface to react with the moisture in air and this creates a mobile surface layer. Depolarizing effects were also observed with the BGO crystals. However, due to the ruggedness of the crystal, the crystal could be cleaned simply. After cleaning with acetone the depolarizing effects were no longer observed. Indications are that in BGO cleaning is required only on a monthly basis.

CENTER, INC.

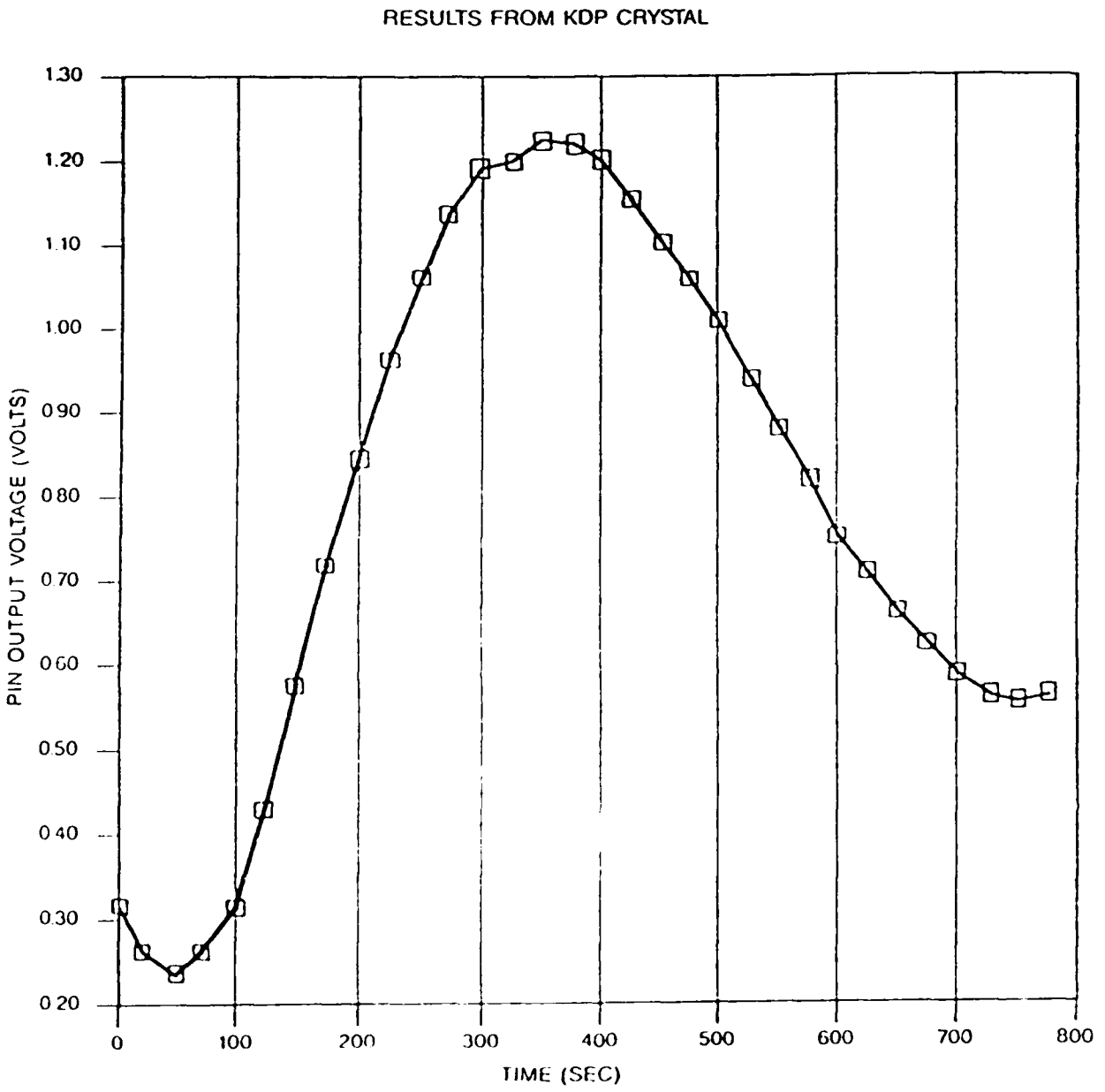

Figure 18. Observed output fluctuations in KDP crystal. No electric field applied.

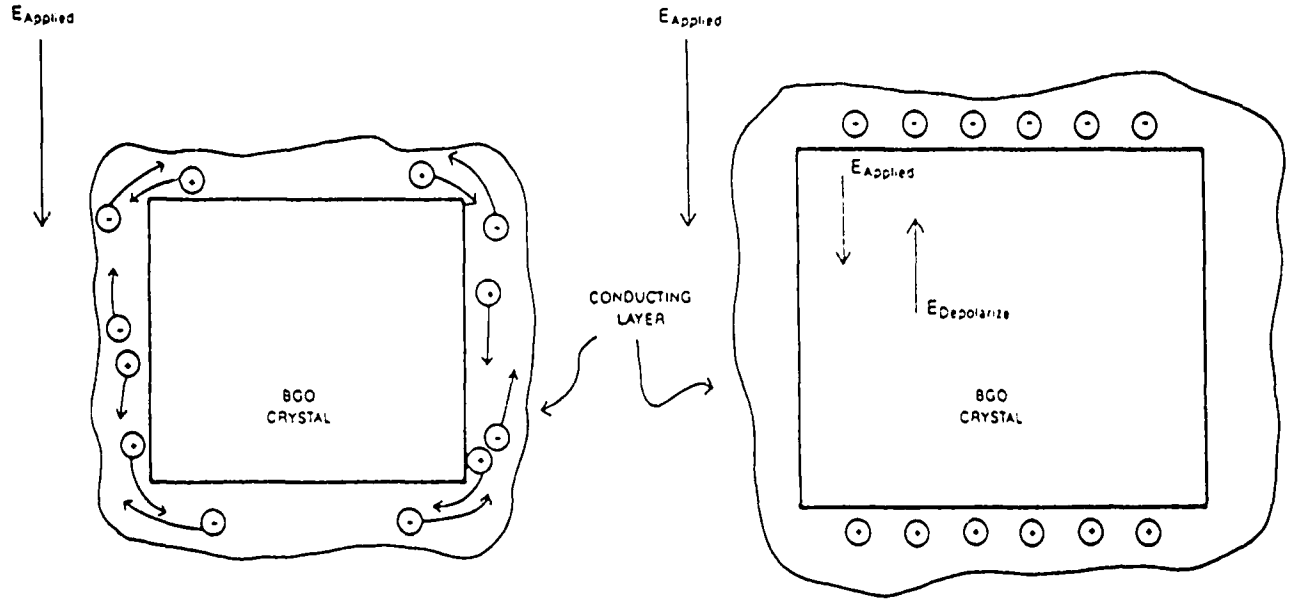

a) Immediately after field turned on.

b) Equilibrium situation.

Figure 19. Depolarization effect.

In conclusion, KDP electro-optic crystals are not a viable crystal choice for an electric field sensor. By contrast, the behavior of BGO is consistent and reliable. It displays linear response over a large range. The upper and lower extents of this sensing range were not determined explicitly. On the upper end the air began to break down at around 1.2×10^6 V/m limiting our ability to test the crystal at larger D.C. voltages. On the low end, fields as low as 2×10^2 V/m were measured. With improved photodetectors/amplifiers, which are easily developed fields of approximately 1 V/m, should be measurable with a 10 mm or 20 mm BGO crystal. The BGO crystal exhibits excellent directional sensitivity. This directional sensitivity makes the crystal quite useful for developing a 3 axis sensor system capable of measuring electric field strength and direction. BGO is an excellent candidate for a viable electro-optic crystal for developing a fiber optic D.C. electric field sensor.

3.3.2.2 A.C. Measurements

In addition to D.C. measurements which were done to measure the effect of crystal length on sensor linear sensing range, A.C. measurements were also made. The objective in the A.C. measurements was to determine the feasibility of using the BGO crystal as a sensing element in a fiber optic electric field sensor for lightning research. This sensor must be capable of making measurement of large, pulsed fields. Values for electric fields of interest in this research area are 3×10^6 V/m in a μs time period. In addition the crystals must be rugged enough to survive a direct discharge since the crystals may be exposed to direct hits. From the discharges observed in the D.C. measurements, the BGO is clearly rugged enough.

In order to show feasibility in this area, GEO-CENTERS, INC. used a transformer driven spark gap device to generate a ramp voltage which peaks at 2.5×10^4 V in 1.2 μs. This ramp is followed by exponentially damped ringing. The period of the ringing is about 100 ns. The pulse is shown in Figure 20. Here a Tektronix high voltage probe attached across the pulse generator's terminals was used to provide a signal for the storage scope. This pulse has the characteristics necessary to test the feasibility of the BGO crystal for lightning research applications.

The ellipsometer configuration for the A.C. measurements was the same as that used for the D.C. measurements. Avalanche Photo Diodes (APDs) were used as detectors since they have large gain and high bandwidth capabilities. GEO-CENTERS, INC. has two APDs. APD 1 has a bandwidth of 100 MHZ, while the other, APD 2, has a bandwidth of 10 MHZ. Both of these APDs are capable of tracking the 1.2 μs ramp. Only APD 1, however, is suitable for measuring the ringing phenomenon. One of the output polarizations was focussed into an optical fiber which was used to transmit the output light to a different room for these experiments. Only then was the APD sufficiently shielded from the radiation given off by the pulse generating equipment. This experimental set-up is shown in Figure 21.

The APDs electrical output was monitored on a Tektronix 7623A storage oscilloscope with a 7A18 dual trace amplifier plug-in and a 7B85 delaying time base plug-in. A scope camera was used to record the data on film for later analysis.

The initial experiments were done with the 5 mm BGO crystals. The ellipsometer was set up to ensure sensitivity to fields in the

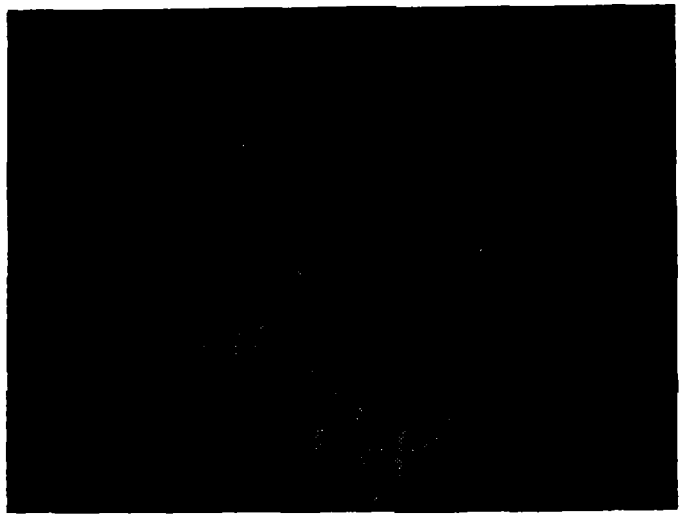

Figure 20. Voltage applied to the parallel plates.
Verticle scale arbitrary units.
Horizontal scale 200 nsec./Div.

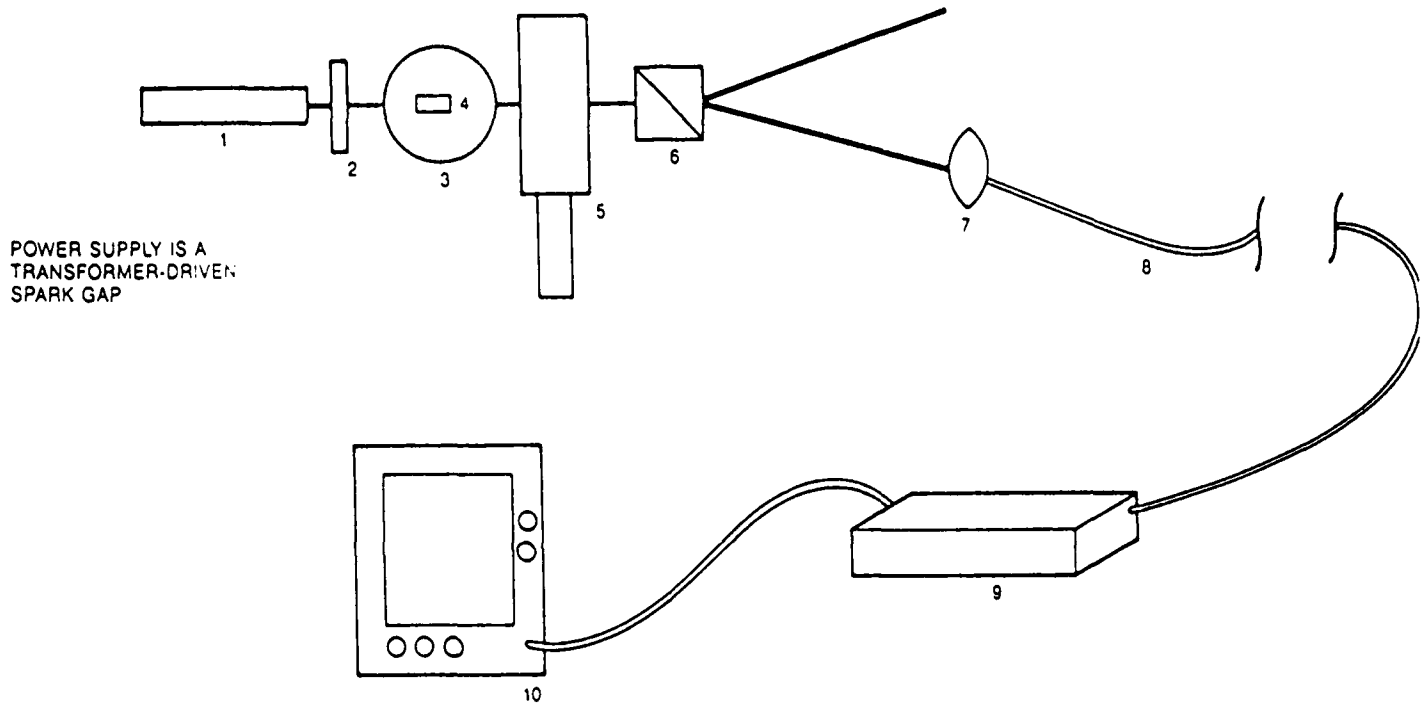

1) HeNe LASER (5 mW)
2) LINEAR POLARIZER
3) TEST PLATES
4) CRYSTAL
5) LINEAR COMPENSATOR
6) WOLLASTON PRISM
7) OBJECTIVE LENS
8) OPTICAL FIBER
9) AVALANCHE PHOTO-DIODE (A P D)
10) STORAGE OSCILLOSCOPE

Figure 21. Experimental setup for AC measurements.

<001> direction only. Correspondingly, the fields were only applied in that direction. For these experiments, APD 2 was used. The results are shown in Figure 22. The upper trace is the sensor's response. The lower trace is the high voltage probe's response. Clearly the sensor is following the ramp voltage. In addition, the ringing is shown, indicating that the sensor tracks field oscillations with 100 ns period. The reliability of the sensor is demonstrated by Figure 23. This figure shows the superposition of 5 traces from 5 different applied pulses.

Next the linearity of the system under these conditions was tested using APD 1. Since this APD is A.C. coupled, in order to get the optical biasing information necessary to insure maximum sensitivity and to allow for the calculation of changes in transmission, a beam chopper was used to make the nominally steady state transmission an A.C. signal. The optical biasing results are shown in Figure 24a and 24b. Figure 24a shows the maximum optical power available, Figure 24b indicates the optical biasing. The biasing is at about one-half maximum power. The results from two trials are tabulated in the Table 2 below:

TABLE 2

Optical Biasing Information

	V_{bias}	V_{max}	nominal bias
trial 1	.7V	1.1V	64%
trial 2	.6V	1.1V	55%

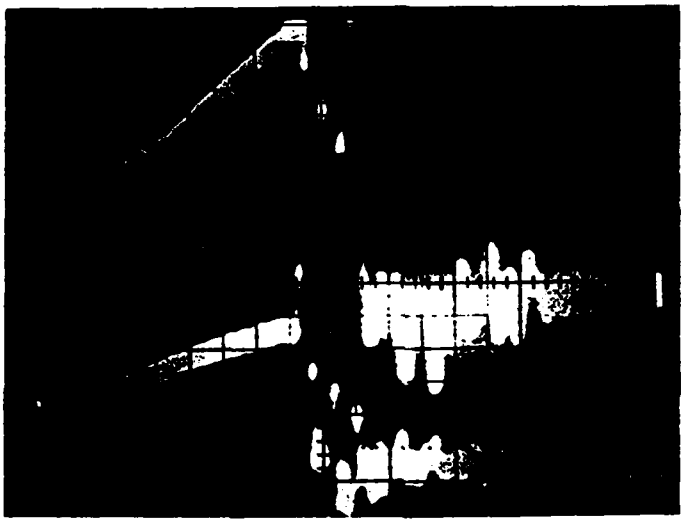

Figure 22. Sensor's response to pulsed electric fields. The upper trace is the sensor's response. The lower trace is the response of a Tektronix's high-voltage probe.

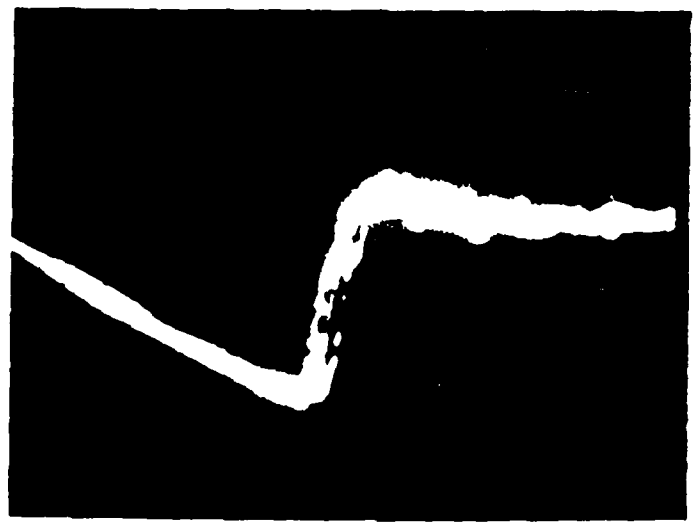

Figure 23. Results from five superimposed tests.
Verticle scale arbitrary units.
Horizontal scale 200nsec./Div.

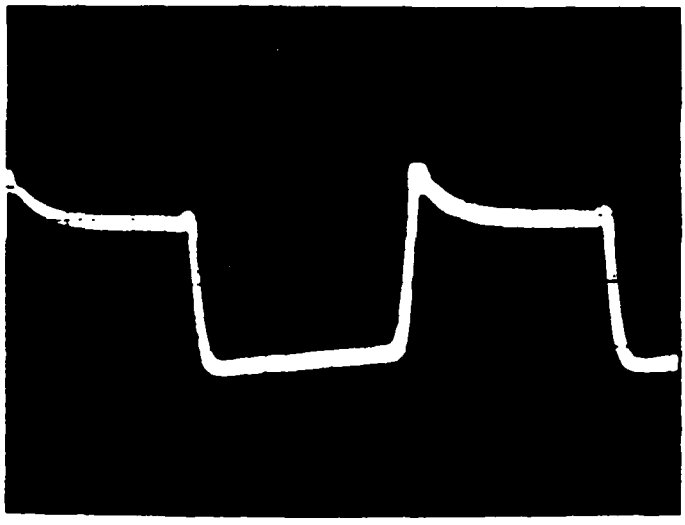

a) Maximum optical power.

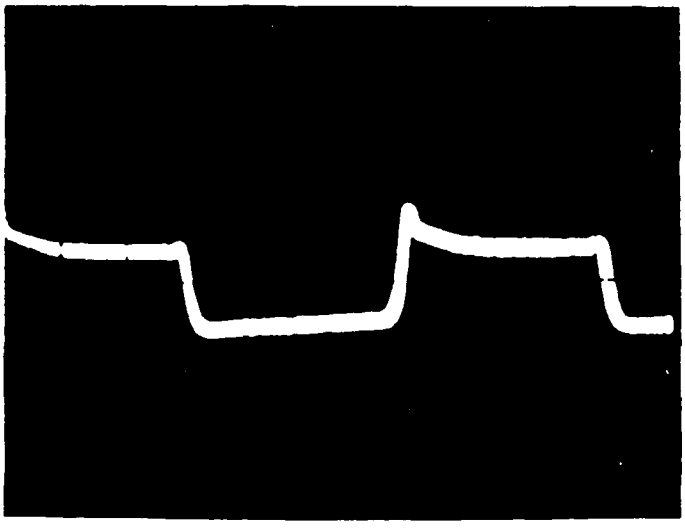

b) Biasing approximately ½ maximum.

Figure 24. Representative optical biasing information.

Ideal optical biasing would result in a nominal bias of 50%, but the biasing shown in Table 2 is adequate for preliminary measurements.

Two different pulse magnitudes were used and the electric fields were applied in both the <001> and the <00$\bar{1}$> directions. The pulse magnitudes were 2.5×10^6 V/m and 1.25×10^6 V/m. This change was created by changing the capacitor plate spacing. In each case, the pulse length is about 1μs. The sensor's response to the different pulses can be seen in Figures 25a, 25b, 26a, and 26b. Numerical results are tabulated below along with change in transmission values:

TABLE 3

Tabulated Results from A.C. Electric Field Measurements

Applied Electric Field (V/m)	% Transmission Change
$+ 2.5 \times 10^6$	9.8
$+ 1.25 \times 10^6$	3.6
$- 1.25 \times 10^6$	-5.3
$- 2.5 \times 10^6$	-9.1

The linearity of the sensor is demonstrated by the fact that the change in transmission approximately doubles when the applied field is doubled. In addition, reversing the applied field polarity reverses the sign of the transmission change. Deviations from a linear response are most likely due to changes in the nominal optical biasing, which occur when the applied electric field amplitude was changed.

a) Electric field applied in positive direction.

b) Electric field applied in negative direction

Figure 25. 5 mm sensor's response to electric field pulse.
Verticle scale 0.5 Volts/Div.
Horizontal scale 0.2 μsec./Div.
Applied field = $2.50 \cdot 10^6 (\frac{V}{m})$

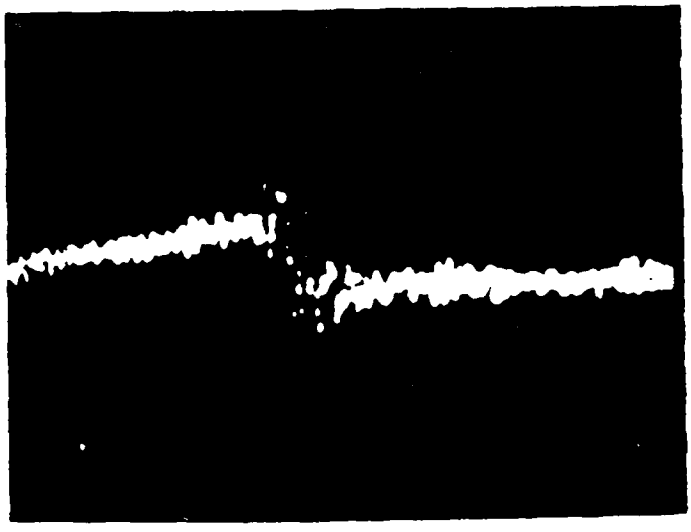

a) Electric field applied in positive direction.

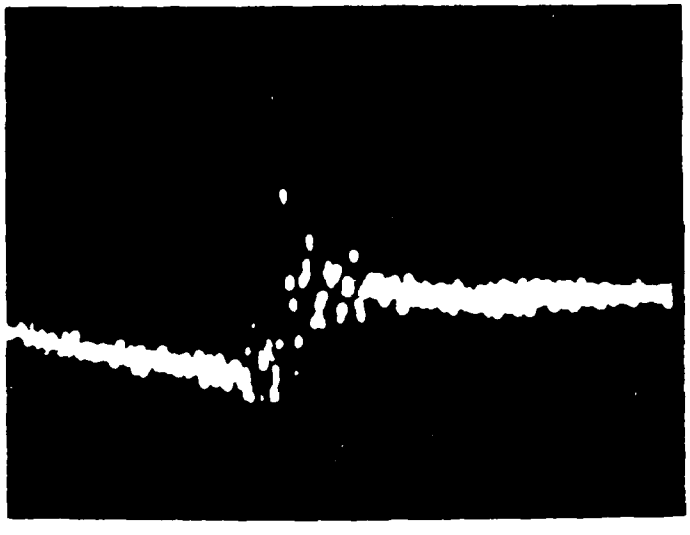

b) Electric field applied in negative direction.

Figure 26. 5mm sensor's response to electric field pulse.
Verticle scale 0.5 Volts/Div.
Horizontal scale 0.2 μsec./Div.
Applied field $1.25 \cdot 10^6$ (V/m).

As described in Section 3.2, the sensor's induced birefringence is proportional to the length of the crystal, the longer the crystal incorporated, the more sensitive the device. However, because of the finite velocity of light, if the crystal gets too long, the response of the sensor will no longer follow a quickly changed field faithfully. To explore the limitations of crystal length and bandwidths, different length crystals were used to measure quick pulses. The first pulse keyed on was the 1 μs ramp pulse. The results are shown in photographs taken of the storage scope screen, Figures 27a, 27b and 27c. Note that for each crystal length, the traces exhibit the same characteristics of a ramp down followed by an abrupt return to zero and decaying oscillations. Clearly, all these lengths introduced no significant distortion of the 1 μs pulse. In addition, all crystals followed the ringing phenomenon.

As predicted, the 20 mm crystal exhibited the largest transmission change, while the 5 mm crystal exhibited the smallest. The changes in transmission are tabulated below:

TABLE 4

The Effects of Crystal Length on A.C. Measurement Response

Crystal Length	% Transmission
20 mm	35
10 mm	17.5
5 mm	7.5

These values confirm the predicted linear relationship between change in transmission and crystal length. A crystal length of

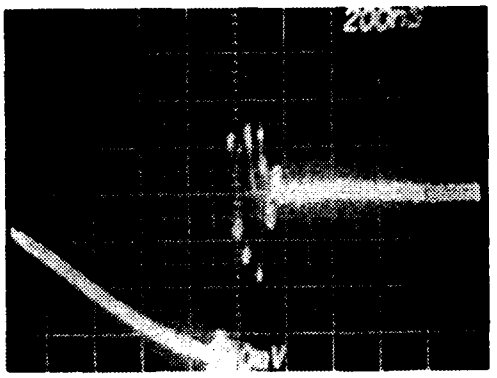

a) 20 mm Crystal —

200 $\frac{mV}{Div}$ at $\frac{200\ ns}{Div}$

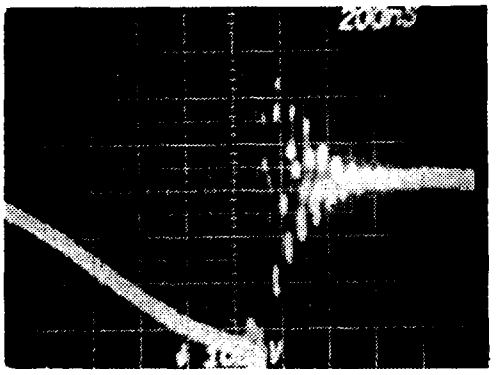

b) 10 mm Crystal —

100 $\frac{mV}{Div}$ at $\frac{200\ ns}{Div}$

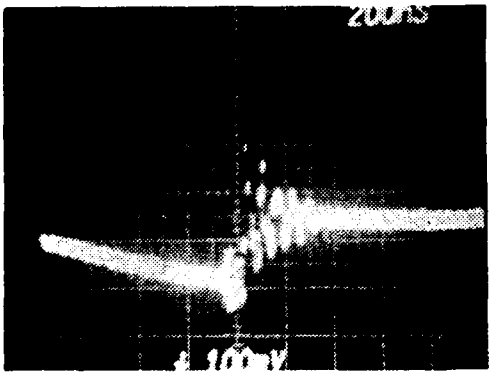

c) 5 mm Crystal —

100 $\frac{mV}{Div}$ at $\frac{200\ ns}{Div}$

Figure 27. A comparison of the response of different length BGO crystals to the same pulse.

30 mm to 40 mm would still afford linear response with this applied electric field.

Since all the crystals tracked the 1 μs ramp portion of the pulse, the ability of a crystal to track the ringing phenomenon was investigated since its period of oscillation is much less than 1 μs. The results of this test are shown in Figures 28a and 28b. Note that though the sensor and probe are not completely in phase, both the 20mm and 10mm crystals track the ringing phenomena. This response is also greater for the 20mm crystals as is predicted.

The excellent sensitivity to the applied electric field shown by the 20 mm crystal suggested that this crystal would be applicable for small field measurements. Success in these tests opens up new areas for applications for the fiber optic electric field sensor. To simulate small fields, a B and K Precision 3020 Sweep/Function Generator was used to supply voltage to the plates. This function generator is capable of supplying 20 volts. Using the plates with 1 cm spacing gives a field of only 2×10^3 V/m. The frequency of the applied field was set at 1 KHz. The PIN Diode Circuit used previously in the DC measurement portion of the experiments was used as the detector.

The results of these tests are shown in Figures 29a, 29b, 29c, and 29d. Clearly, this crystal is feasible for use in an electric field sensor for measurement of these low fields (1×10^3 V/m). Similar results were also achieved with the 10 mm crystal but with the expected reduction in transmission change. The detection system used was not sufficiently sophisticated to eliminate the ripple noise. This same field was measured using two of these PIN diode detectors; one for each polarization state. When the two outputs were put into a differencing amplifier, the

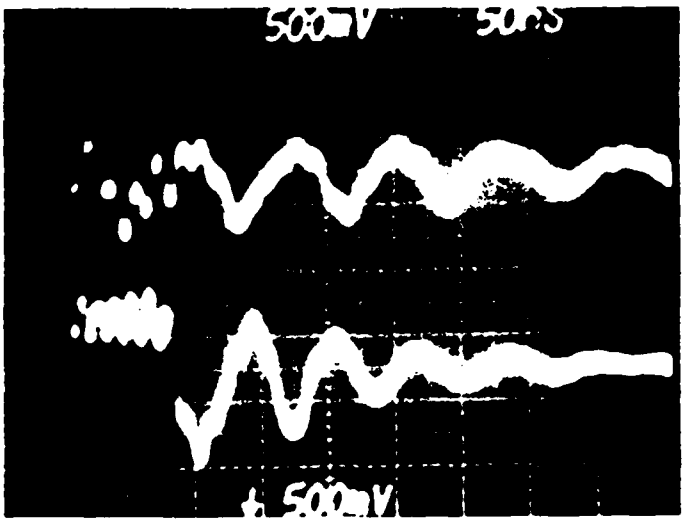

a) 20 mm crystal

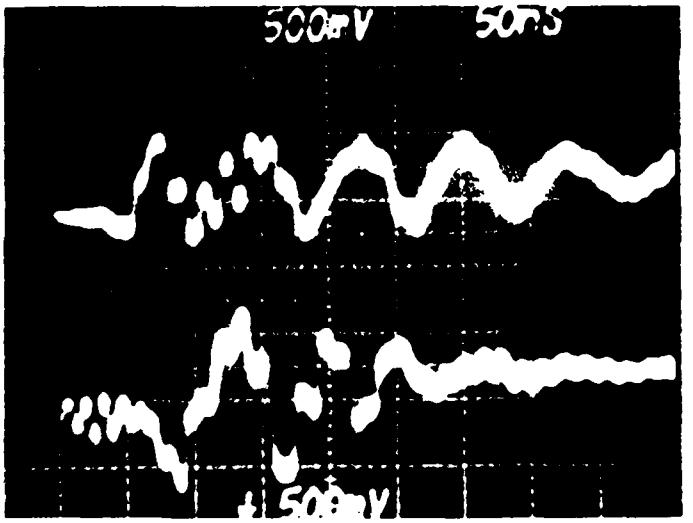

b) 10 mm crystal

Figure 28. Sensor and probe response to applied pulse.
Sensor's response compared to the high-voltage probe's response.
In each case, the trace from the high-voltage probe is on the top.

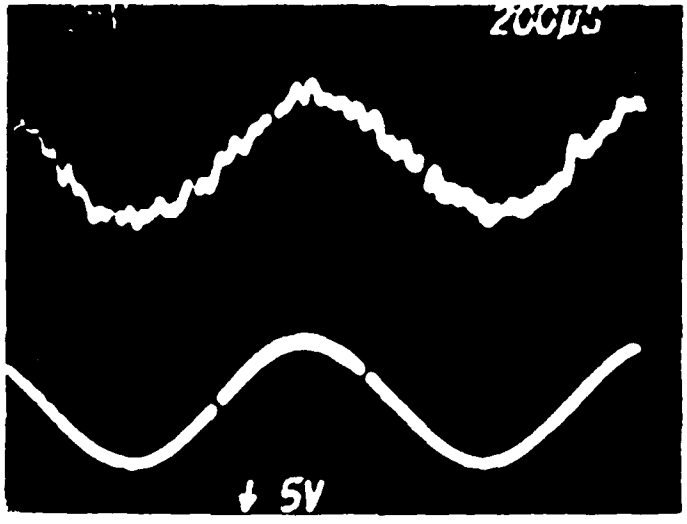

a) Field parameters $1 \cdot 10^3 \frac{V}{m}$ at 2 kHz

b) Field parameters $1 \cdot 10^3 \frac{V}{m}$ at 2 kHz

Figure 29. 20 mm crystal's response to low-level oscillating fields. In each case, the upper trace is the crystal's response, while the lower trace is the signal generator output.

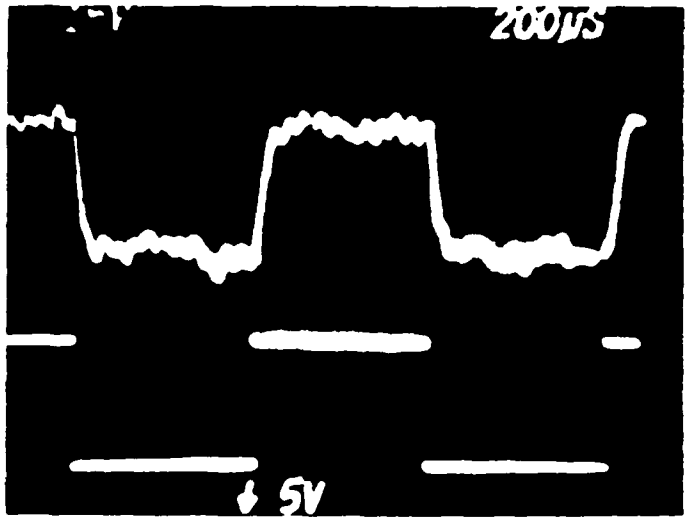

c) Field Parameters $1 \cdot 10^3 \frac{V}{m}$ at 2 kHz

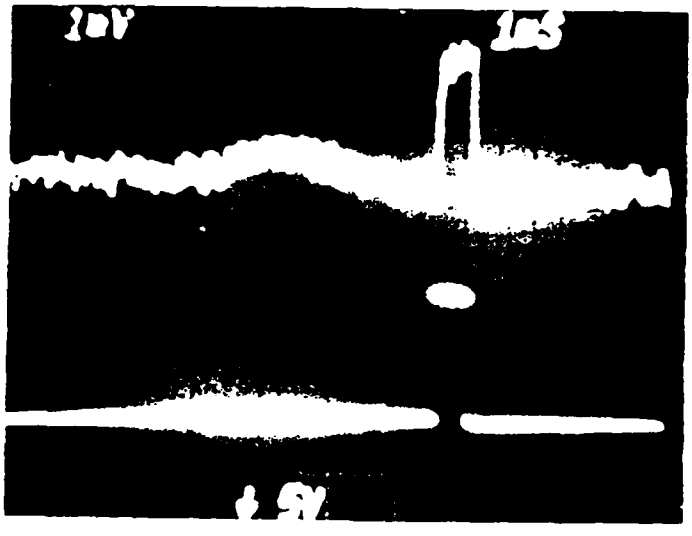

d) Field Parameters $1 \cdot 10^3 \frac{V}{m}$ at 500 μs Pulse Width

Figure 29. 20 mm crystal's response to low-level oscillating fields. In each case, the upper trace is the crystal's response, while the lower trace is the signal generator output.

random noise was eliminated. The result is a system capable of detecting even smaller fields. With this set up, a field of approximately 200 V/m was measured. Indications are that a field value of less than 1 V/m should be measurable with a 20 mm crystal at the shot noise limit of the incorporated photodiode.

The results of the A.C. tests indicate the feasibility of developing an electric field sensor which is capable of measuring electric fields between 1 V/m and $1x10^7$ V/m. A.C. measurement bandwidth capability of greater than 100 MHz should be possible with this technology. In addition, there would be no need to integrate this sensor's output signal to determine the applied electric field. This makes a fiber optic electric field sensor based on the electro-optic effect in BGO a unique sensor whose capabilities make it well suited to lightning research applications.

3.3.3 Results from Tests at AFWAL/FIESL Facility

Between December 10 and December 12, 1985, GEO-CENTERS, INC. personnel tested a prototype fiber optic electric field sensor based on the electro-optic effect with personnel of the Air Force Wright Aeronautical Laboratory's (AFWAL) Lightning Research Group at their facility. This electric field sensor was fabricated at GEO-CENTERS' Boston Laboratory facility. For electric field measurements (A.C.) a photodetector with high speed amplifier (10 MHz) was interfaced to the output of the fiber optic electric field sensor.

The sensor was fabricated using a 2 mm x 3 mm x 5 mm BGO crystal with the following dimensions:

$\langle 110 \rangle$ = 2 mm

$\langle \bar{1}10 \rangle$ = 5 mm

$\langle 001 \rangle$ = 3 mm

The polaroids for the sensor were oriented so that the sensor was sensitive only to applied electric fields in the $\langle 001 \rangle$ crystal direction. The A.C. measurement bandwidth capability of the sensor and its associated electronics was approximately 10 MHz, with the photodetector amplifier being the limiting component. This sensor was designed for the measurement of very large electric fields (1×10^7 V/m) as the crystal length ($\langle \bar{1}10 \rangle$) was comparatively short.

At the AFWAL/FIESL facility in Dayton, Ohio, the sensor's response to four different electric field types was measured. In all of the tests a voltage was applied to two circular plates with a plate spacing of approximately one inch. The maximum electric field which we were able to introduce was limited by the electrical breakdown of the air between the two parallel plates.

The first test type involved a pulsed electric field. The applied voltage pulse was negative with a peak voltage of approximately -24,000 volts and a pulse duration of approximately 5 to 6 μs. With plates with one inch spacing, this results in an applied peak electric field of approximately 9.5×10^5 V/m.

The second test type involved an oscillatory applied electric field. The maximum applied voltage in this case is approximately 9,300 volts, and the oscillatory period was approximately 9 μs with the amplitude of the applied voltage decreasing after each successive period. This results in a peak applied electric field of the order of $\pm$ 3.7×10^5 V/m.

The third test type involved the electric field produced by charging the parallel plates with the power supply and then rapidly discharging them with a grounding strap. For these tests, the plates were charged with a voltage of approximately 26,000 volts, producing a field of approximately $1x10^6$ V/m. This was the largest electric field produced during any of these tests.

The fourth test type involved an oscillatory field similar to that mentioned above. In this case, the power supply's voltage was increased until the parallel plates broke down. This produces a very rapid initial pulse followed by the oscillatory type field previously discussed. This test was predominantly performed to characterize GEO-CENTERS, INC.'s photodetector system's A.C. bandwidth capability.

In order to evaluate the prototype fiber optic sensor, it was placed between the two parallel plates to which the voltage was applied. A He-Ne laser was used as the optical source for the fiber optic electric field sensor for these tests. This source was chosen as it provided the greatest incident optical intensity to the fiber optic sensor. This source, however, did present some difficulty as a plasma oscillation in the laser discharge produced a modulation in the He-Ne laser's output intensity at a frequency of approximately 1.5 MHz. It should be noted that if a new He-Ne laser (the He-Ne used was about 5 years old and has subsequently deteriorated) was employed as the optical source, the plasma oscillation would be completely eliminated. This modulation was approximately 1/16th of the amplitude of the total optical intensity which was input to the fiber optic sensor. This modulation prevents "clean" output signal detection of small changes in the transmitted optical intensity. Through integration of the sen-

sor's output, a signal with excellent signal to noise is achieved as the effect of the modulation at 1.5 MHz is averaged out. This allows for the detection of low level changes in the optical transmission with this optical source.

The sensor output was monitored by an avalanche photodiode/amplifier whose output was recorded by a Data Precision transient recorder. In addition to the sensor's output, the employed transient recorders were used to monitor the applied current to the parallel plates and the applied voltage across the parallel plates.

Figure 30 shows results from one of the pulsed field tests. The upper trace is the applied voltage to the parallel plates. The middle trace is the response of the fiber optic sensor to the electric field pulse. The lower trace is the integral of the fiber optic sensor's response. The sensor's output clearly tracks the input voltage pulse. The integration of the sensor's output shows that the sensor's signal to noise ratio is actually quite good, as the change in the integral of the sensor's output signal is easily discerned. In the absence of the 1.5 MHz noise, the sensors output should show the same or better signal to noise ratio as compared to the integrated sensor output allowing for electric field measurements to be made without signal integration.

Figure 31 shows the results from an oscillatory electric field test. The upper trace is the applied current to the plate. The second trace is the fiber optic sensor's response to the applied electric field. The third trace is the integrated fiber optic sensor's response. The lower trace is the integral of the applied voltage to the parallel plates. A comparison of the applied current and the fiber optic sensor's response shows that

CENTERS, INC

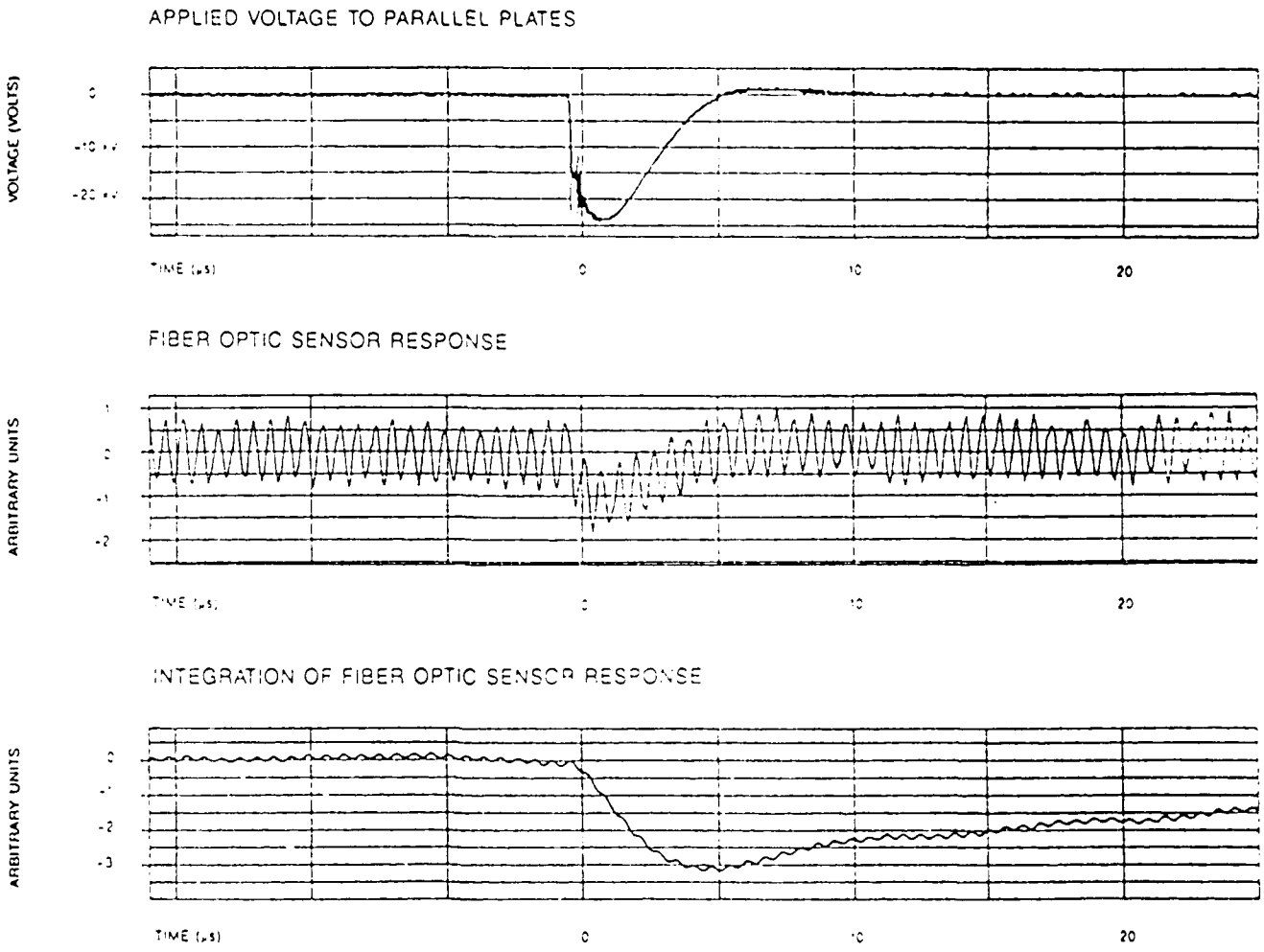

Figure 30. Fiber optic sensor's response to a pulsed electric field.

the phase relationship between current and voltage in a capacitor is clearly observable. The current and voltage in a capacitor are related by:

$$i = C \frac{dV}{dt} \tag{30}$$

The applied current in this case is clearly a damped sinusoid. Therefore, the voltage should be 90^{o} out of phase with respect to the applied current ($\frac{d}{dx} \sin x = \cos x$), as the electric field is related to the applied voltage by:

$$E = \frac{V}{d} \tag{31}$$

where:

d = the plate spacing

Therefore, the applied electric field is in phase with the applied voltage. The 90^{o} phase difference between the applied current and fiber optic sensor's response to the applied electric field is clearly observed in the top two traces. Furthermore, the integration of the sensor's response to the applied electric field and the integration of the applied voltage are both shown to be in phase with the applied current. These data clearly show that the prototype fiber optic electric field sensor is capable of measuring electric fields. The integrated sensor response follows the integral of the applied voltage excellently. The applied electric field change from the final valley to the final peak for this test was approximately 2×10^{5} V/m. The sensor still tracks this electric field change with a good signal to noise ratio. By incor-

GEO CENTERS, INC

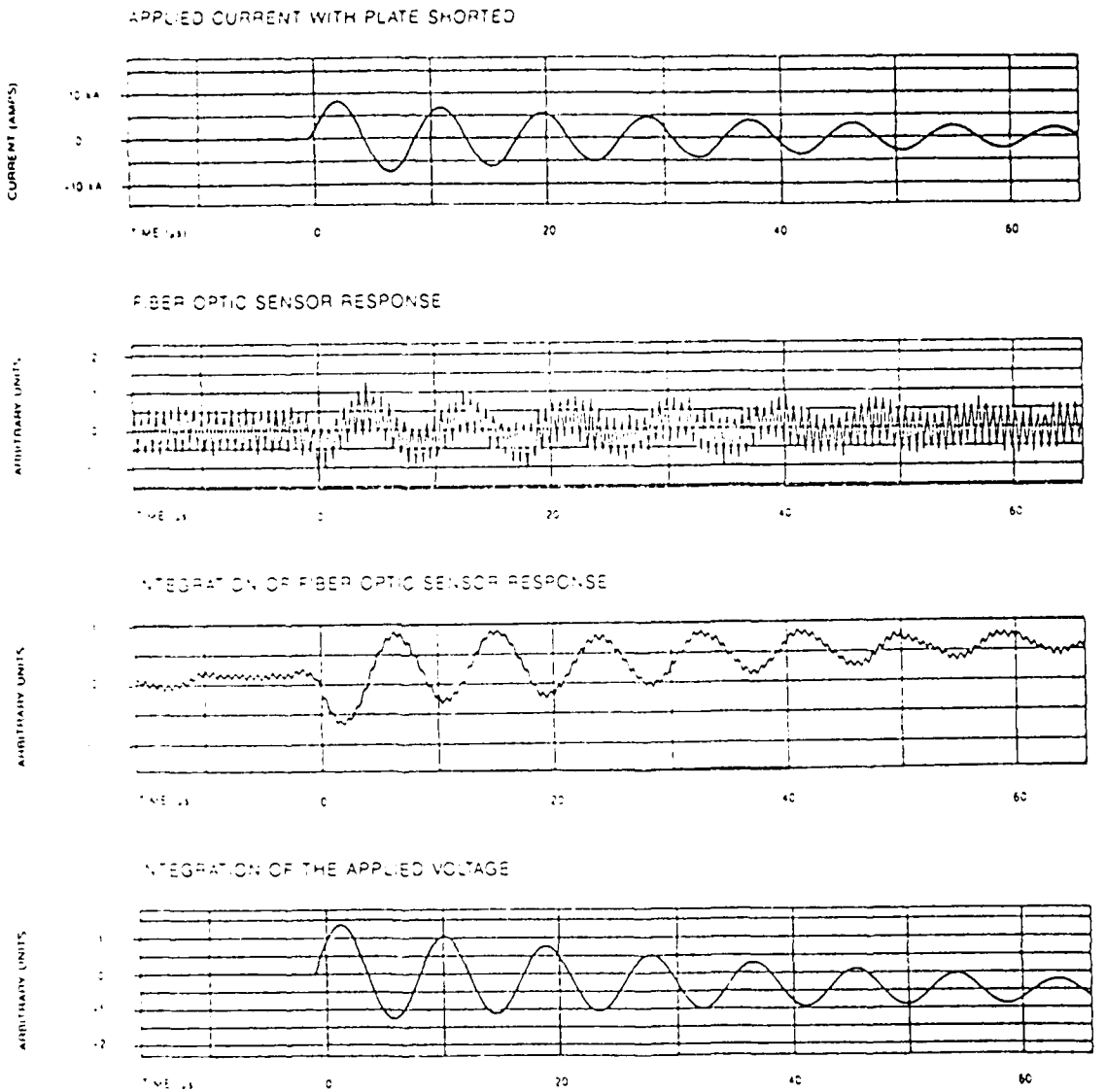

Figure 31. Fiber optic electric field sensor's response to an oscillatory field.

porating a newer optical source, the signal to noise ratio could be significantly improved with the existing sensor. If a crystal of longer length is employed further improvements in the signal to noise ratio would be observed.

Figure 32 shows the results of one of the tests where the charged parallel plates were rapidly discharged with a grounding strap. The top trace is the fiber optic sensor's response to the parallel plate discharge. The bottom trace is the integrated fiber optic sensor's response. The sensor responds quite well to this type of electric field. Even though the initial rise time is at approximately the same frequency as the 1.5 MHz oscillation, with an electric field of this amplitude ($1x10^6$ V/m) the signal to noise ratio is sufficient to track the input electric field. Integration of the sensor's output, once again, shows a signal with improved signal to noise ratio. The comparatively slow fall time in these tests is due most likely to the capacitance and resistance in the cables and power supplies.

Figure 33 shows results from the test which was used to characterize the A.C. measurement bandwidth capability of the avalanche photodiode/amplifier system used for output detection in the fiber optic electric field sensor. For this experiment the three curves shown were recorded from three separate tests. These tests were run with the electric field generating equipment set up as it was for the oscilitory field test, except in this case the power supply voltage was increased until the air between the parallel plates broke down. The top trace shows the response of the AFWAL/FIESL system which was used to monitor the applied voltage to the plates. This system converts the measured voltage to an optical signal, transmits the signal to the data recording station on an optical fiber, and then reconverts the optical

CENTERS, INC

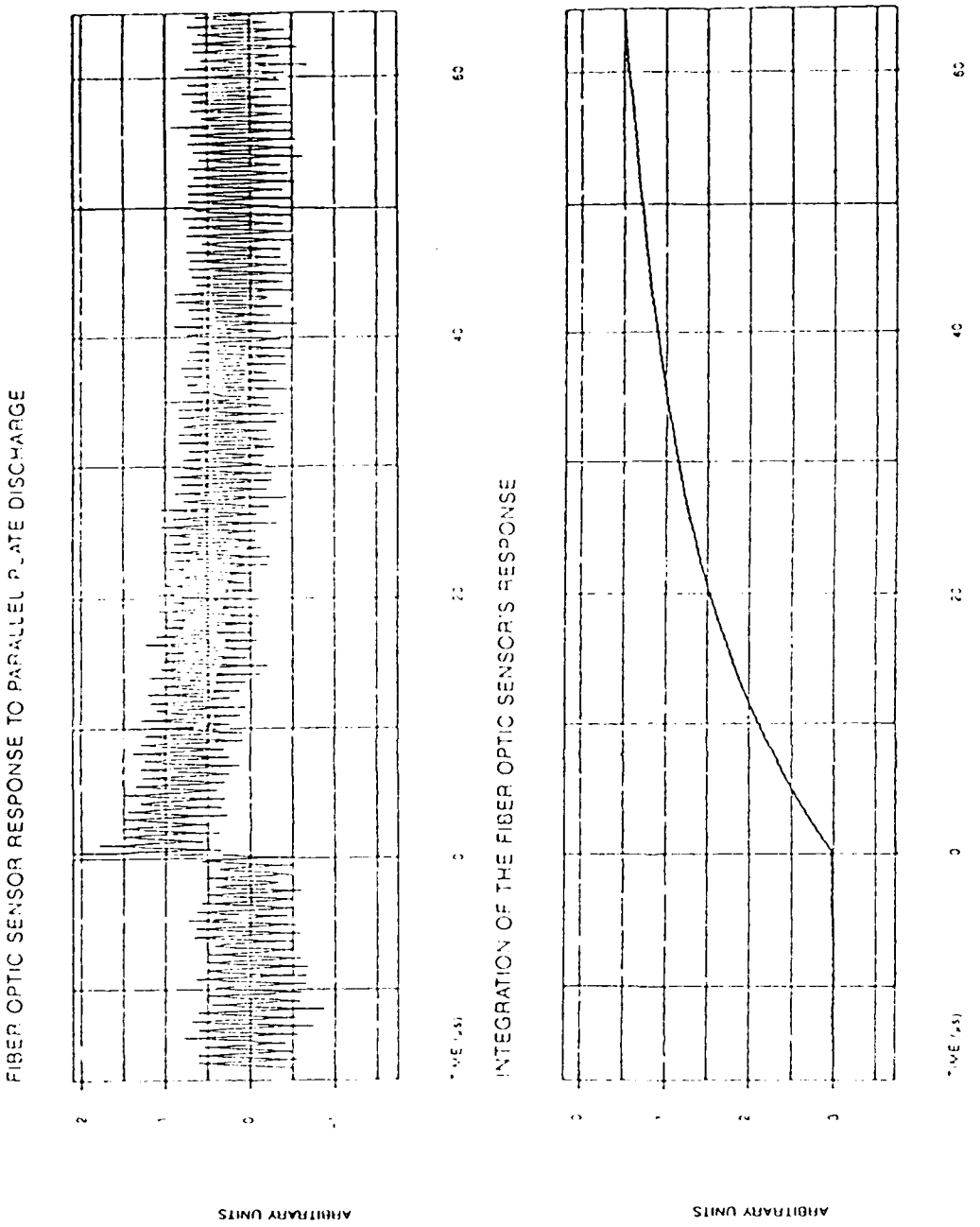

Figure 32. Fiber optic sensor's response to parallel plate discharge.

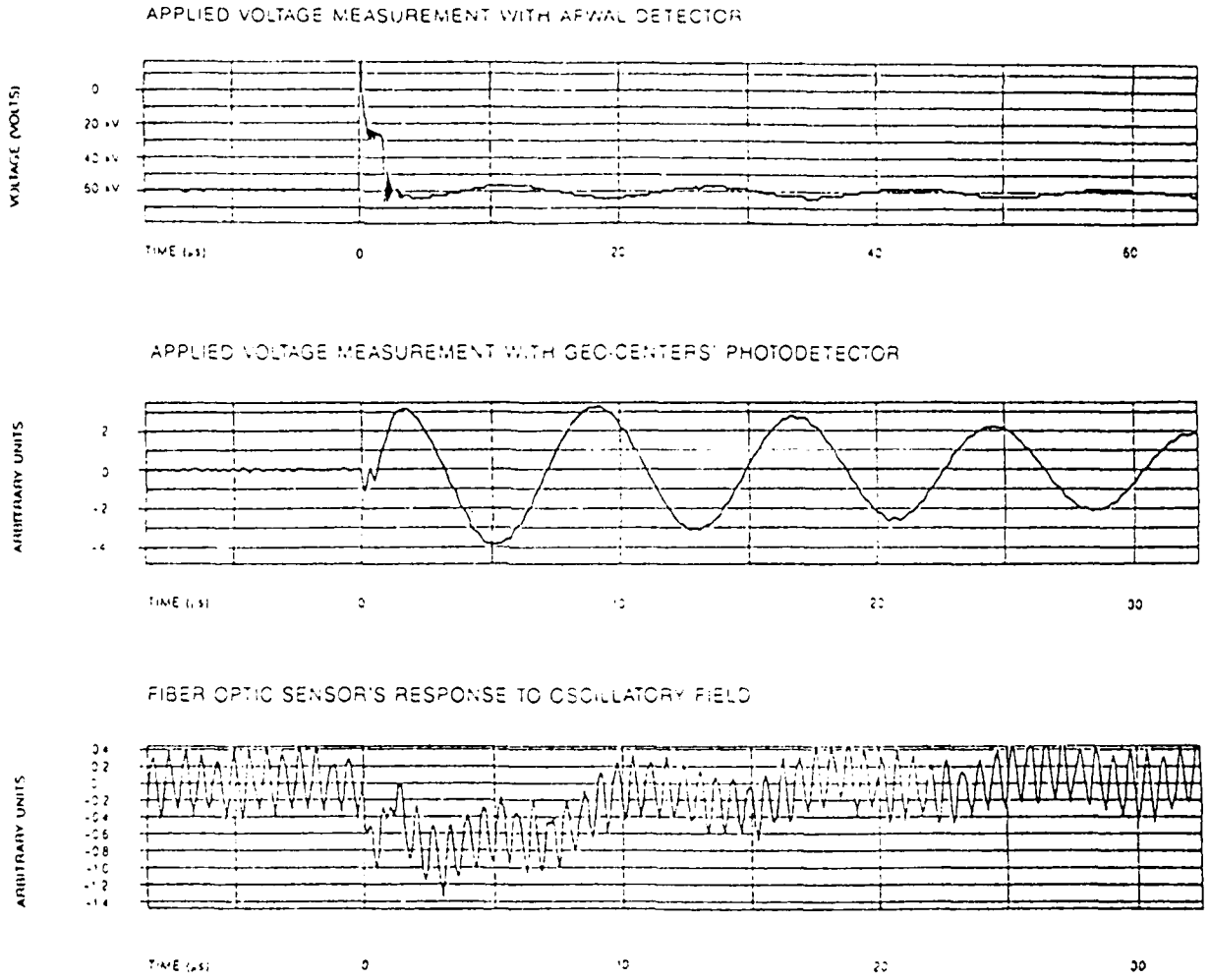

Figure 33. Results from test to characterize GEO-CENTER's photodetector system.

signal to an electrical signal with a photodetector/amplifier. The middle trace is the result of connecting the optical output of the AFWAL/FIESL system to GEO-CENTERS' avalanche photodiode/amplifier system for optical to electrical converison. The bottom trace is the fiber optic sensor's response to this type of applied electric field. The AFWAL/FIESL photodetector/amplifier clearly tracks the change in voltage which occurs at the point where air breakdown occurs. The much slower oscillations are also tracked by this photodiode/amplifier system. GEO-CENTERS' avalanche photodiode/amplifier system with its 10 MHz bandwidth capability does not accurately track this initial rapidly changing signal. It does, however, track the sinusoidal oscillations quite well. The fiber optic sensor signal shows the same bandwidth limited behavior when responding to the initial air breakdown as that of the AFWAL optical output and the GEO-CENTERS' detector. This test shows that the fiber optic sensor's response to A.C. applied electric fields was limited by the measurement bandwidth capability of the avalanche photodiode/amplifier system. This detector amplifier was chosen because, even though it is limited in its A.C. measurement bandwidth capability, it has larger responsivity (volts/watt) than any photodetector system that was available at GEO-CENTERS. GEO-CENTERS plans to develop avalanche photodiode/amplifier systems with higher A.C. measurement bandwidth capability with the equivalent responsivity of this system.

This series of tests shows that the technology developed at GEO-CENTERS, INC.'s Boston Laboratory facility with bulk optics can be utilized in a fiber optic sensor. At GEO-CENTERS tests were performed with a 5mm long BGO crystal with pulsed fields of between $1x10^6$ V/m and $3x10^6$ V/m and a pulse duration of approximately 1 μs. With electric fields of this amplitude, the 1.5 MHz laser plasma oscillations do not prevent the clean detection of

the optical transmission change. At the AFWAL facility this conclusion was confirmed with the tests performed with the parallel plate discharge (see Figure 32), where an electric field amplitude change of $1x10^6$ V/m occurred. The change in optical transmission with applied electric field was similar with both the bulk optics and fiber optic sensor configurations. With an improved source and photodetector, an electric field sensor with improved small electric field ($<<1x10^5$) measurement capability and very high A.C. measurement bandwidth capability will be realized. This can be accomplished by incorporating a new He-Ne laser as an optical source and incorporating high bandwidth circuitry in the photodetector amplifier. Future fiber optic electric field sensors applicable for use by the AFWAL/FIESL lightning research group will employ longer crystals. This will result in a larger induced birefringence in the crystal as a function of the applied electric field. Work at GEO-CENTERS' Laboratory described in this report indicates that a sensor with a linear sensing range between 1 V/m and $1x10^7$ V/m and an A.C. measurement bandwidth capability in excess of 100 MHz should be achieved in a fiber optic sensor which incorporates a 10 mm BGO crystal.

4.0 Conclusions & Recommendations

The Phase I non-invasive electromagnetic field sensor program initiated the development of a fiber optic electric field sensor based on the electro-optic effect. During the Phase I research effort, attention went to determining the best electro-optic crystal and crystal geometry for developing a sensor with measurement capabilities applicable to both lightning and NEMP research. The Phase I research effort investigated the effect of electro-optic crystal type and electro-optic crystal geometry on a sensors's linear sensing range and A.C. bandwidth measurement capabilities. In addition, electro-optic crystal physical properties such as ruggedness, dielectric permeability, and the temperature dependence of its electro-optic coefficients were investigated in order to assure the development of a practical sensor. The data collected during the Phase I research effort indicate $Bi_4(GeO_4)_3$ (BGO) is an excellent electro-optic crystal for the development of a fiber optic electric field sensor for both lightning and NEMP research.

The data generated during this research effort demonstrate a linear sensing range with a 10 or 20 cm long BGO crystal of $1x10^2$ V/m to $1x10^7$ V/m. By incorporating an additional stage of amplifiers in our detection electronics, a linear sensing range of 1 V/m to $1x10^7$ V/m should be easily realized. In addition, in all experiments performed to date, the photodetector/ amplifier system and not the electro-optic crystal limited the A.C. measurement bandwidth capability of the sensor/electronics system. Still, an A.C. measurement bandwidth capability in excess of 10 MHz was demonstrated during the Phase I research effort. By incorporating high bandwidth circuitry in a photodetector system, an A.C. measurement bandwidth capability which approaches a GHz should be realized.

Theoretical calculations which were done during the Phase I research effort indicated a unique capability of electro-optic cyrstals with 23 and $\bar{4}3m$ point group symmetries. These calculations showed that by cutting the crystal along certain axes and by incorporating two optical axes and polarizer orientations, a single crystal can be used to create two independent electric field sensors with orthogonal directional sensitivities. This affords the possibility of creating a sensing head with 3 axis electric field sensitivity by utilizing only two electro-optic crystals. This allows for the development of an electric field sensor capable of measuring electric field strength and direction at a significant cost reduction, when compared to an electric field sensor which incorporates three electro-optic crystals. This is the first time that this result has been reported. Consequently, GEO-CENTERS, INC. will investigate the filing of a patent.

The design, fabrication, and testing of a prototype fiber optic electric field sensor based on the electro-optic effect was accomplished during the Phase I research effort. The work performed shows that the technology developed in this research effort with bulk optics can be successfully utilized in a fiber optic sensor. This portion of the Phase I research effort is an important step to the development of a fiber optic electric field sensor for lightning research, as it clearly shows the feasibility of utilizing this technology for electric field measurements. In the proposed next phase of this research effort, sensors will be developed which have the measurement capabilities of the $\dot{D}$ sensors, which are presently incorporated in lightning research.

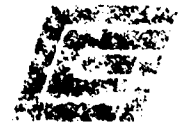

In order for a fiber optic electric field sensor to realize its full A.C. measurement bandwidth capability, a photodetector system with an A.C. measurement bandwidth capability which approaches a GHz needs to be developed. This bandwidth capability is achievable in a photodetetor amplifier system which incorporates discrete components and not operational amplifiers which are presently used. The development of photodetector amplifier systems with this capability should occur in a Phase II research effort. This would result in an electric field sensor which has as high an A.C. measurement bandwidth capability as any other available electric field sensor.

The Phase I research experimental effort determined the effect of electro-optic crystal length on the linear sensing range of a fiber optic sensor. These data allow the design of specific electric field sensors for particular measurement requirements based on empirical data. Because of this, GEO-CENTERS, INC. is now capable of designing specific electric field sensors for lightning, NEMP, and other research areas.

In conclusion, during the Phase I research effort, each of the tasks outlined in the Phase I Statement of Work was successfully completed. In addition to meeting these objectives, a prototype fiber optic electric field sensor was fabricated at GEO-CENTERS Boston Laboratory and tested in conjunction with members of the Air Force Wright Aeronautical Laboratories Lightning Research group. This research effort will provide the technical foundation for the future development of fiber optic electric field sensors for lightning and NEMP research applications.

Appendix A

Analysis of the transverse electro-optic effect in KDP.

The calculation showing a transverse electro-optic effect in KDP proceeds much like the calculation for BGO which is done explicitly in the text.

After a $\pi/4$ rotation about the <001> direction, the indicatrix equation becomes

Equation I

$$1 = \frac{1}{n_{o1}^2}(x_1'^2+x_2'^2) + \frac{1}{n_{o3}^2}x_3'^2 + \frac{2}{\sqrt{2}}r_{41}[A_1\varepsilon_-(x_1'x_3'+x_2'x_3') + A_2\varepsilon_+(x_1'x_3'-x_2'x_3')] + r_{63}(x_1'^2+x_2'^2)$$

where:

$$A_i = \frac{E_i}{|\vec{E}_{tot}|}$$
$$\varepsilon_- = (E_1'-E_2')$$
$$\varepsilon_+ = (E_1'+E_2')$$

For light propagating in the x_2' direction, this reduces to

Equation II

$$1 = \frac{1}{n_{o1}^2} + r_{63}E_3' \; x_1'^2 + \frac{1}{n_{o3}^2}x_3'^2 + \frac{2r_{41}}{\sqrt{2}}(A_1\varepsilon_- + A_2\varepsilon_+)x_1'x_3'$$

As before, the indices of refraction for the normal modes are given by the eigenvalue of Equation II. For the case, E applied along the <001> direction, the eigenvalues are

$$\frac{1}{n'^2} = \frac{1}{n_{o1}^2} + r_{63}E_3 \text{ and } \frac{1}{n'^2} = \frac{1}{n_{o3}^2}$$

The corresponding eigenvectors are $\begin{bmatrix}1\\0\end{bmatrix}$ and $\begin{bmatrix}0\\1\end{bmatrix}$, respectively. Using Equation 16 from the text to calculate the birefringence, gives

$$\Gamma_{in} = \frac{L}{\lambda} n_{o1}^3 r_{63}E$$

For E- applied along the <110> direction

$$\frac{1}{n'^2} = \frac{\left(\frac{1}{n_{o1}^2} + \frac{1}{n_{o3}^2}\right)}{2} \pm \frac{\left(\frac{1}{n_{o1}^2} - \frac{1}{n_{o3}^2}\right)}{2\cos\alpha}$$

where:

$$\alpha = \tan^{-1}\left(\frac{2r_{41}E}{\left(\frac{1}{n_{o1}^2} - \frac{1}{n_{o3}^2}\right)}\right)$$

EO CENTERS, INC

The corresponding non-normalized eigenvectors are:

$$\begin{bmatrix} 1 \\ \left(\frac{1}{n_{o1}^2} - \frac{1}{n_{o3}^2}\right)\left(\frac{1}{2} + \frac{1}{2\cos\alpha}\right) \\ r_{41}E \end{bmatrix} \quad \text{and} \quad \begin{bmatrix} \left(\frac{1}{n_{o1}^2} - \frac{1}{n_{03}^2}\right)\left(\frac{1}{2} - \frac{1}{2\cos\alpha}\right) \\ r_{41}E \\ 1 \end{bmatrix}$$

The induced birefringence is

$$\Delta n = \frac{\pi L}{\lambda}\left[\frac{n_{o1}^3}{2}\left(\frac{1}{n_{o3}^2}-\frac{1}{n_{o1}^2}\right)\left(1-\frac{1}{2\cos\alpha}\right) - \frac{n_{o3}^3}{2}\left(\frac{1}{n_{o1}^2}-\frac{1}{n_{o3}^2}\right)\left(1-\frac{1}{2\cos\alpha}\right)\right]$$

For E-field applied along the $\langle\bar{1}10\rangle$ direction the indices of refraciton remain n_{o1} and n_{o3}. This situation exhibits KDP's natural birefringence of

$$\Delta n_{nat} = \frac{\pi L}{\lambda}\left(\frac{1}{n_{o1}^2} - \frac{1}{n_{o3}^2}\right)$$

GEO-CENTERS, INC

References

1. Shibata, K., "A Fiber Optic Electric Field Sensor Using the Electro-Optic Effect of $Bi_4Ge_3O_{12}$," Fuji Electric Corporate Research and Development, Ltd., Japan (Presented paper preprint).

2. Kyuma, K., Tai, S., Nunoshita, M., Mikami, N., and Ida, Y., "Fiber-Optic Current and Voltage Sensors Using a $Bi_{12}GeO_{20}$ Single Crystal," Journal of Lightwave Technology, Vol. LT-1, No. 1, March 1983.

3. Ihara, S., et. al., "The Development of BSO/Fiber-Optic Magnetic Field and Voltage Sensors," Sumitomo Electrical Technical Review," Number 23, January 1984, pages 175-183.

4. Hamasaki, Y., Gotolt, H. Katoh, M., Takeuchi, S., "OPSEF: An Optical Sensor for Measurement of High Electric Field Strength," *Electronics Letters, Vol. 16, No. 11, pp.* 406-407, 1980.

5. Filter, W., Landron, C., Muron, D., "Photonic Measurement of Microwave Pulses," Presented at SPIE: Fiber Optic and Laser Sensors; Conference 566, August 22, 1985.

6. Trinks, H., Matz, G., Shilling, H., "Electro-Optic System for EMP Measurements," IEEE Trans. Electromag. Compat., Vol. EMC-22, No. 1, pp. 75-77, 1980.

7. Massey G., Johnson, J., and Erickson, D., "Laser Sensing of Electric and Magnetic Fields for Power Transmission Applications," SPIE Vol. 88 Polarized Light, pp. 91-96, 1976.

GEO-CENTERS INC.

U.S. Government Printing Office: 1986 [illegible]

END

12-86

DTIC